


Spring 1-1-2017

Effect of Hydration and Confinement on Micro-Structure of Calcium-Silicate-Hydrate Gels

Harish Kumar Gadde

University of Colorado at Boulder, harish.gadde@colorado.edu

Follow this and additional works at: https://scholar.colorado.edu/cven_gradetds

 Part of the [Civil Engineering Commons](#), [Construction Engineering Commons](#), and the [Nanoscience and Nanotechnology Commons](#)

Recommended Citation

Gadde, Harish Kumar, "Effect of Hydration and Confinement on Micro-Structure of Calcium-Silicate-Hydrate Gels" (2017). *Civil Engineering Graduate Theses & Dissertations*. 88.
https://scholar.colorado.edu/cven_gradetds/88

This Thesis is brought to you for free and open access by Civil, Environmental, and Architectural Engineering at CU Scholar. It has been accepted for inclusion in Civil Engineering Graduate Theses & Dissertations by an authorized administrator of CU Scholar. For more information, please contact cuscholaradmin@colorado.edu.

**Effect of Hydration and Confinement on Micro-Structure of Calcium-
Silicate-Hydrate Gels**

by

Harish Kumar Gadde

M.Tech, Structural Engineering, SASTRA University, 2014

A thesis submitted to the
Faculty of the Graduate School of the
University of Colorado in partial fulfillment
of the requirement for the degree of
Master of Science

Civil, Environmental and Architectural Engineering Department

2017

This thesis entitled:
Effect of Hydration and Confinement on Micro-Structure of Calcium-Silicate-
Hydrate Gels

written by Harish Kumar Gadde

has been approved for the Civil, Environmental and Architectural Engineering Department

Dr. Mija H. Hubler

Dr. Yunping Xi

Dr. Wil V. Srubar

Date_____

The final copy of this thesis has been examined by the signatories, and we find that both the content and the form meet acceptable presentation standards of scholarly work in the above mentioned discipline.

Gadde, Harish Kumar (M.S., Civil Engineering)

Study on the Effect of Hydration and Confinement on Micro-Structure of Calcium-Silicate-Hydrate Gels

Thesis directed by: Dr. Mija H. Hubler

Calcium-silicate-hydrate(C-S-H) gel is a primary nano-crystalline phase present in hydrated Ordinary Portland Cement (OPC) responsible for its strength and creep behavior. Our reliance on cement for infrastructure is global, and there is a need to improve infrastructure life-times. A way forward is to engineer the cement with more durability and long-term strength. The main purpose of this research is to quantify the micro-structure of C-S-H to see if cement can be engineered at various length scales to improve long-term behavior by spatial arrangement. We investigate the micro-structure evolution of C-S-H in cement as a function of hydration time and confinement. Scanning electron microscopy (SEM) and Energy Dispersive X-ray Spectroscopy (EDS) were used to quantify the material and spatial properties of C-S-H as a function of hydration time. The data obtained from these experiments was used to identify C-S-H phases in cement sample. Pair Distribution Function (PDF) analysis of HD C-S-H phase with different hydration times was done at Advanced Photon Source, Argonne National Laboratory, beamline 11-ID-B. Only nonlinear trends in the atomic ordering of C-S-H gel as a function of hydration time were observed. Solid state ^{29}Si Nuclear Magnetic Resonance (NMR) was used to quantify the effect of confinement on two types of C-S-H: white cement C-S-H and synthetic C-S-H. NMR spectra revealed that there is no significant difference in the structure of

C-S-H due to confinement when compared with unconfined C-S-H. It is also found that there is significant difference in the Si environments of these two types of C-S-H. Though it does seem possible to engineer the cement on atomic scales, all these studies reveal that engineering cement on such a scale requires a more statistically accurate understanding of intricate structure of C-S-H than is currently available.

ACKNOWLEDGEMENT

I would first like to thank my thesis adviser Dr. Mija H. Hubler of Civil, Environmental and Architectural Engineering Department, University of Colorado Boulder. I would like to express my sincere gratitude to Dr. Hubler for her patience, brain storming ideas and guiding me from first day to last day. It's been an enlightening experience working with her.

I would also like to thank my defense committee members: Dr. Yunping Xi and Dr. Wil V. Srubar for their valuable inputs and comments on my thesis. Without their passionate participation and inputs, my learning would have been incomplete.

I would like to thank Tomoko Borsa at Nanomaterials Characterisation Facility(NCF), University of Colorado Boulder for training me on various techniques in Scanning Electron Microscopy(SEM) and Energy Dispersive Spectroscopy(EDS) which helped me to gain knowledge on SEM spectroscopy. I would also like to thank Karena W. Chapman, Olaf J. Borkiewicz, Kevin A. Bryer for their assistance during the PDF Analysis at beamline 11-ID-B, Advanced Photon Source(APS). I would also like to acknowledge Paul Boni of Geological Sciences department for making SEM samples. I would also like to thank Fred Luiszer of Laboratory of Environmental and Geological studies(LEGS) for characterizing the samples for Nuclear Magnetic Resonance(NMR) studies. I would like to thank Jeremy Zhong of Intertek Laboratories for conducting the solid state ^{29}Si NMR experiments.

I must thank my parents and sister for always believing, encouraging in every aspect of my life and being there when I needed them the most. Without them I could not have come this far in life. My friends for their continuous support and encouragement in every step of my life.

This research used resources of the Advanced Photon Source, a U.S. Department of Energy (DOE) Office of Science User Facility operated for the DOE Office of Science by Argonne National Laboratory under Contract No. DE-AC02-06CH11357.

Author
Harish Kumar Gadde

CONTENTS

CHAPTER

I.	INTRODUCTION	
	1. Project motivation	1
	2. Approach.....	2
	3. Outline of Thesis	4
II.	LITERATURE REVIEW	
	1. Formation of C-S-H gel	5
	2. Structural Analogies of C-S-H	7
	3. Morphology and Layered Feature of C-S-H	11
	4. Density & Water Content in C-S-H.....	15
	5. Models of C-S-H.....	16
III.	SCANNING ELECTRON MICROSCOPY	
	1. Introduction.....	23
	2. Sample Preparation	23
	3. SEM Imaging Procedure.....	28
	4. Results	29
	5. Discussion.....	31
IV.	ENERGY DISPERSIVE SPECTROSCOPY	
	1. Introduction.....	32
	2. EDS Experimental Procedure.....	33
	3. Results	34

4. Discussion	35
V. Pair Distribution Function Analysis	
1. Introduction	37
2. Sample Preparation	38
3. PDF Experimental Procedure	40
4. Results	42
5. Discussion	44
VI. Nuclear Magnetic Resonance Spectroscopy	
1. Introduction	47
2. Sample Preparation	48
3. Synthesis of C-S-H	48
4. ²⁹ Si NMR Experimental Procedure	50
5. Results	51
6. Discussion	52
VII. Conclusions and Future Work	
1. Overview	54
2. Conclusions from SEM/EDS	55
3. Conclusions from PDF	56
4. Conclusions from ²⁹ Si NMR	56
5. Future Work	57
BIBLIOGRAPHY	59
APPENDIX	62

LIST OF TABLES

Table

3.1 Concrete bulk mount preparation method with diamond suspension.....	27
6.1. ICP-OES characterization.....	50

LIST OF FIGURES

Figure

1.1	Schematic representation of experimentation.....	3
1.2	Experimentation sequence based on different length scales.....	3
2.1	SEM image of C_3S hydration product with hydration time of (a) 1 day (b) 7 days (c) 14 days (d) 30 day.....	6
2.2	Figure representing the hydration process in cement (a) before hydration (b) 10 minutes, (c) 10 hours, (d) 18 hours, (e) 1–3 days, and (f) 2 weeks.....	7
2.3	C-S-H layer showing a main calcium octahedral layer with silicate tetrahedron attached on both sides. Calcium octahedral, Silicate chains and oxygen atoms are shown as light blue, dark blue tetrahedron, and red spheres respectively. P-pairing, B-bridging tetrahedrons.....	8
2.4	Crystal Structure of Tobermorite 11 Å proposed by Hamid. Calcium octahedral, Silicate chains and oxygen atoms are shown as light blue, dark blue tetrahedron, and red spheres respectively.....	8
2.5	Crystal Structure of Tobermorite proposed by Merlino [16]. Silicate chains, calcium octahedral, and oxygen atoms are shown as dark blue, light blue tetrahedron, and red spheres, respectively.....	9
2.6	Crystal Structure of jennite projected along [010] (top) and [100] (bottom). Calcium octahedral, Silicate chains and oxygen atoms are shown as light blue, dark blue tetrahedron, and red spheres respectively. P-pairing, B-bridging tetrahedrons, H-hydroxyl group.....	11
2.7	(a) TEM micrograph showing inner and outer C-S-H in a hardened C_3S paste. White arrows show the boundary layer (b) globules of inner C-S-H. (c) fibrillary structure of outer C-S-H.....	12
2.8	AFM photos of C-S-H particles on a nanoscale.....	13

2.9	X-ray diffraction (XRD) patterns of nano-crystalline C-S-H phases with different Ca/Si ratios. Wavelength=0.95006 Å	14
2.10	TEM photos for the tobermorite and C-S-H. a: A synthesized C-S-H with Ca/Si=0.9, quite similar to the tobermorite structure. b: C-S-H gel with Ca/Si=1.7	14
2.11	Figure representing C-S-H globule with representing change in water content states obtained during drying from 11% RH and rewetting to different RH and again returning to 11% RH	16
2.12	Powers and Brownyard model.....	17
2.13	Jennings colloidal model.....	18
2.14	Relationship between Ca/Si and silicate chain length of tobermorite and jennite based on tobermorite and jennite structure.....	20
2.15	Realistic molecular model of C-S-H. White and blue spheres are hydrogen and oxygen atoms of water molecules respectively. Gray and green spheres represents intra and inter-layer calcium ions respectively. Red and yellow sticks represents oxygen and silicon atoms	22
3.1	a) carbon sputter, b) samples mounted on SEM sample stub.....	28
3.2	JEOL JSM-6480 LV SEM machine at NCF.....	29
3.3	SEM image showing evolution of cement matrix with hydration time.....	30
4.1	EDS analysis of 18 hours sample showing a) Electron image b) EDS spectrum c) Oxygen smart map d) Silicon smart map e) Calcium smart map.....	35
5.1	Principle of PDF.....	38
5.2	C-S-H mapping procedure for extraction representing a) electron image, smart maps of b) Si, c) Ca, d) O, e) total phase map with 1,2,3 representing regions of C-S-H for extraction.....	39
5.3	EDS spot spectroscopy for identifying C-S-H phases representing a) electron image, b) spot 1, c) spot 2, d) spot 3, e) spot 4, f) spot5.....	40
5.4	a) samples filled in kapton tubes, b) samples mounted in sample changer, c) sample changer mounted on sample stage, d) sample mounted in a rotator.....	41
5.5	Evolution of X-ray Pair Distribution Function (PDF) of C-S-H gel as a function of hydration time with r ranging from 0-10 Å°. Bond peaks are represented by dotted lines.....	43

5.6	Plot showing $G(r)$ peak height evolution with hydration time for Si-O, Ca-Si, Ca-O.....	44
5.7	Comparison with Monteiro experimental data.....	45
5.8	PDF of C-S-H gel with r ranging from $2.5-5 \text{ \AA}$ to clearly observe the evolution of peak heights as a function of hydration time.....	46
6.1	a) Buchner funnel system for filtration, b) C-S-H seed after filtration, WCP in kapton tubes of c) $0.0435''$ d) $0.0270''$, C-S-H seed in kapton tubes of e) $0.0435''$, f) $0.0270''$	50
6.2	NMR spectra for WCP confined in kapton tube of size a) $0.0435''$, b) $0.0270''$	51
6.3	NMR spectra for synthetic C-S-H confined in kapton tube of size a) $0.0435''$, b) $0.0270''$	52
7.1	Testing procedure for TEM/liquid cell microscopy.....	58

CHAPTER I

INTRODUCTION

1. Project Motivation

After water, cement is the second most consumed material on earth. More than 3 billion tons of cement is used annually worldwide. Production of cement itself accounts for approximately 9% of CO₂ emission [1]. According to Portland Cement Association(PCA), the U.S used more than 122 million metric tons of Portland cement in 2006 and China used at least 800 million metric tons [2].

“Recent figures from the UK and US on the state of their concrete civil assets speak for themselves: the UK spends £40 billion per year on the repair and maintenance of its ageing infrastructure, while the US is reported to need ~\$3 trillion over a five year period to raise the overall quality of its infrastructure from poor to acceptable” [3].

Producing a sustainable cement without compromising the strength is very important for future generations. A sustainable cement may be achievable by engineering a new cement starting at the molecular scale that would allow for longer structural lifetimes. As Calcium Silicate Hydrate (C-S-H) is the main binding phase in Portland cement, responsible for strength and durability, understanding the micro structure of C-S-H is very important, independent of the macroscopic properties of concrete. C-S-H gel grows during the initial stages of hydration as a soft phase filling the pore space [4]. At a micro-scale, it is easy to modify/control the material and mechanical properties of such a soft material. The growth of C-S-H gel during initial stages of hydration and its mechanical properties have been studied by many researchers. However, they are far from being well understood and an ongoing debate

in this area [5] [4] [6]. Recent molecular simulations suggested that the degree of jamming in C-S-H changes with hydration time. If the stiffness of the C-S-H is experimentally confirmed to derive from the jamming, new mechanical models would become possible. Therefore, understanding the micro-structure and mechanical properties of C-S-H is very important to produce sustainable cement. The main objective of the research is to develop and employ experimentation to quantify the structure of C-S-H on a wide range of properties which would give more insight into its intricate structure.

2. Approach

Fig 1.1 shows the experimentation sequence used in this study. Two control parameters are used to study the sensitivity of structure of C-S-H and as a potential means to control that structure: hydration time and confinement. It is well known that two phases of C-S-H i.e. low dense (LD) and high dense (HD) are developed during hydration. Maps of the development of LD and HD C-S-H were created at different hydration times using Scanning Electron Microscopy (SEM) and Energy Dispersive Spectroscopy (EDS). The same is done on all the samples which gives a clear picture of evolution of C-S-H with hydration time. Confinement is achieved by growing the sample in small Kapton tubes. Pair Distribution Function (PDF) analysis is employed to investigate the effect of hydration time on C-S-H during the initial 7 days of hydration. Confinement is achieved by growing the samples in different size tubes. ^{29}Si Nuclear Magnetic Resonance (NMR) is used to find the evolution of structure of C-S-H in white cement and synthetic C-S-H for two types of confinement.

Fig 1.2 shows different length scales and experimental method adopted on each length scale.

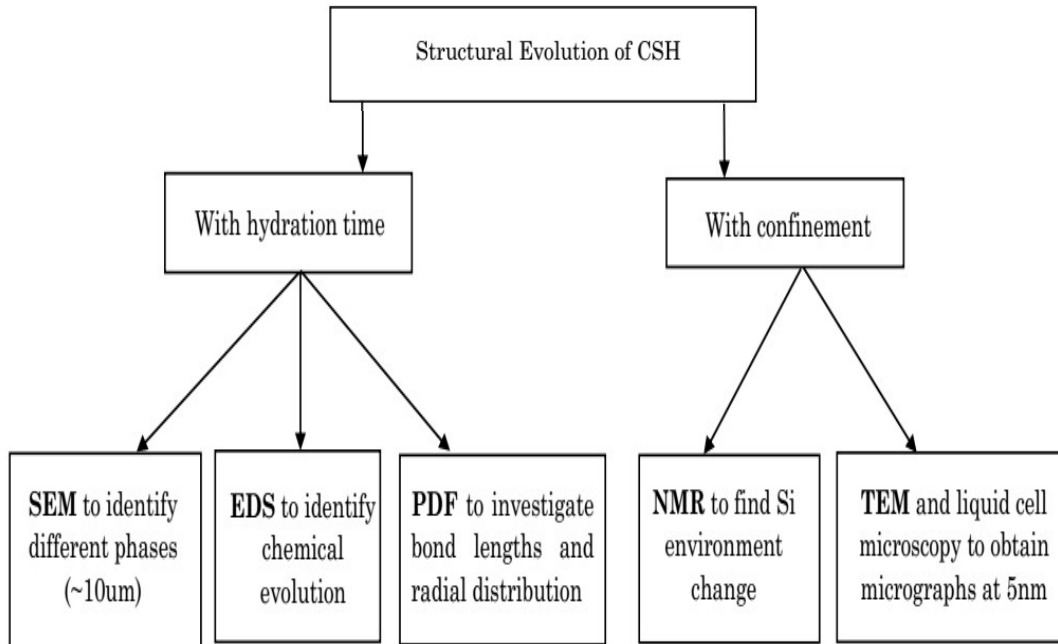


Fig 1.1: Schematic representation of experimentation

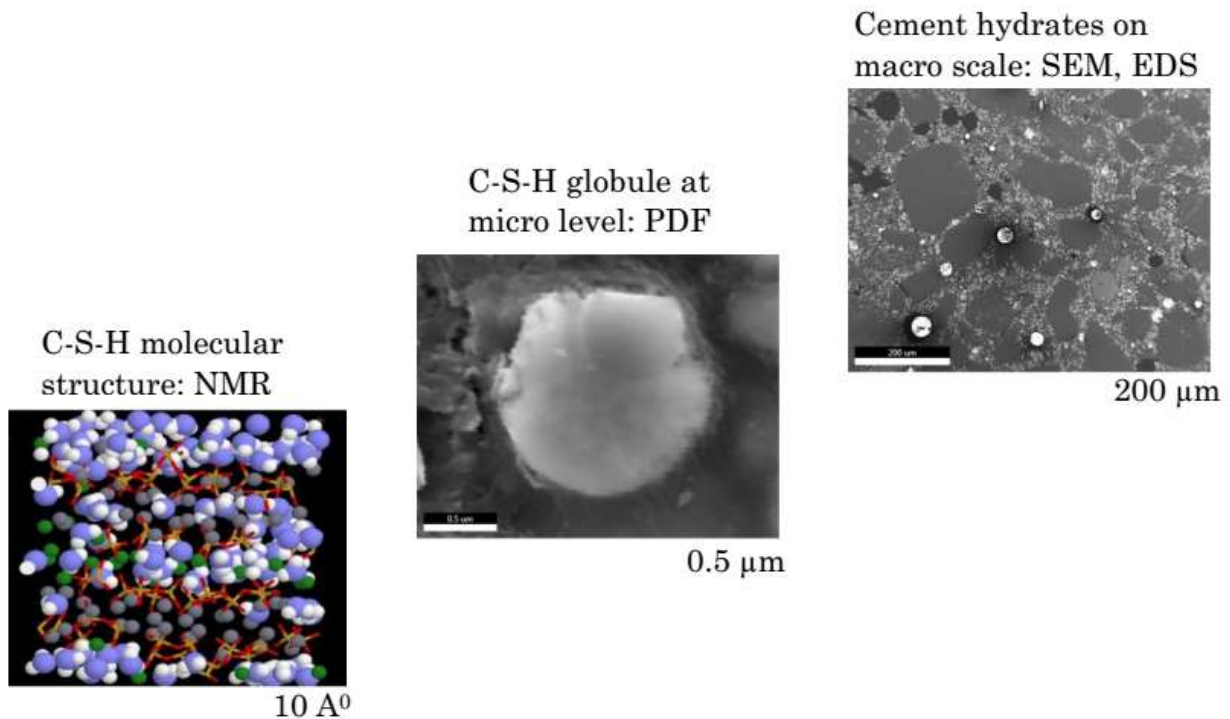


Figure 1.2: Experimentation sequence based on different length scales

3. Outline of Thesis

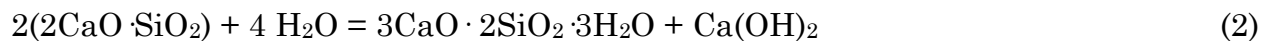
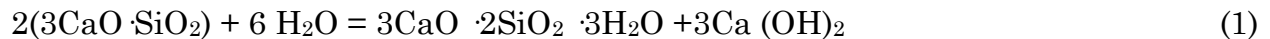
The thesis is divided into 7 chapters. Chapter 1 and chapter 2 give the general introduction to cement and previous studies done on C-S-H, respectively. Chapter 2 reviews the C-S-H models at nano-scale based on both experimental and computational methods. The nano-structure of C-S-H gel and the challenge in model construction are also discussed. Chapter 3 discusses experimental investigation done on cement samples using SEM. Chapter 4 deals with preliminary phase investigation of C-S-H by EDS which is used for sample preparation for PDF analysis. In Chapter 5, PDF analysis of C-S-H phase is discussed. This chapter discusses the radial distribution of atoms, bond lengths and jamming, which can significantly influence the durability of the C-S-H gel with respect to hydration time. This chapter helps to layout a basis for jamming in a cement matrix using confinement. Chapter 6 discusses the quantitative effect of confinement in the early stages of hydration on the evolution of the structure of C-S-H in white cement and synthetic C-S-H using ^{29}Si NMR. Results and discussion are presented in each chapter individually. Chapter 7 presents key conclusions from each study based on all the results. It also provides a link to the previous studies and future scope to investigate and engineer cement using present-day nano-technology.

CHAPTER II

LITERATURE REVIEW

1. Formation of C-S-H gel:

When dry cement powder reacts with water, hydration occurs. There are four major compounds present in cement: di-calcium silicate (C_2S), tri-calcium silicate (C_3S), tetra-calcium alumino-ferrite (C_4AF) and tri-calcium aluminate (C_3A) [7]. Needle-shaped crystal ettringite is the hydration product for aluminate phase. C_3S and C_2S accounts for over 80% of weight of cement and they are responsible for the main hydration product in cement. C_3S is responsible for early strength development in cement in the first month. C_2S reacts slowly and it is responsible for long-term strength development in cement. C_3S and C_2S react with water as shown in Eq. (1) and Eq. (2) to form calcium-silicate hydrate gel and calcium hydroxide.



C-S-H is the principle hydration product in cement and it occupies more than 60% of the structural component in the cement paste. C-S-H is responsible for the strength, shrinkage and durability of the Portland cement concrete [7]. However, due to diversity of the Ca/Si ratio and structural water content, the real composition of the C-S-H gel is not as simple as proposed in the chemical formulas. Morphology evolution of C_3S with hydration time can be seen from Fig 2.1. Some hydration products are formed on the outer surface of original C_3S particles. There are mainly

three different kinds of morphology: (i) the rectangular-like one with clear edges and corners, which are the crystal of calcium hydroxide, (ii) bundles of fibrillar-like one and (iii) ball-like one [8]. The diversity of the morphologies implies the complicity of C-S-H structure.

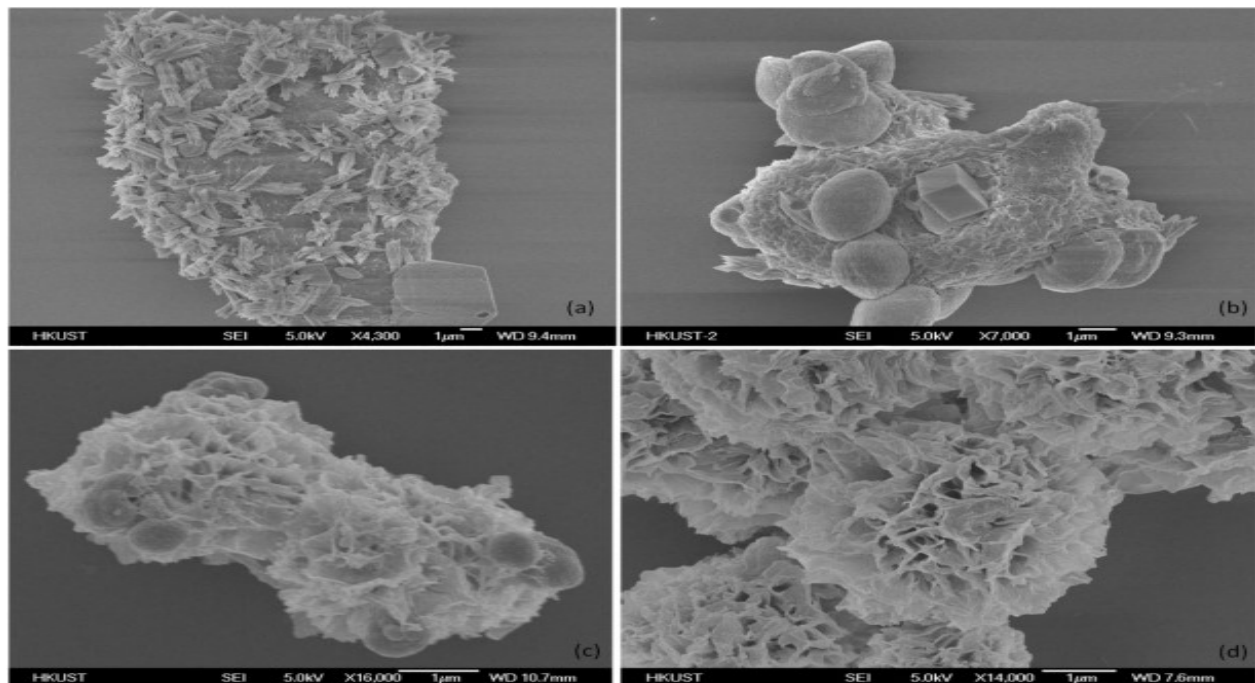


Fig 2.1: SEM image of C_3S hydration product with hydration time of (a) 1 day (b) 7 days (c) 14 days (d) 30 days [8]

Even though the composition and the structure of C-S-H gel have not been comprehensively understood, the cement hydration kinetic is well known [9]. During the hydration in first few minutes, C_4AF reacts with gypsum to form short ettringite rods and an amorphous gel on the outer surface of the cement grains. After the initial reaction, hydration slows down and the induction period starts. Subsequently, the acceleratory period follows the induction period. During 3-24 hours period, almost 30% of the particles present in cement reacts to form C-S-H gel and calcium hydroxide. Growth of C-S-H occurs in 2 phases. After 10 hours hydration, C-S-H

grows from the short ettringite rods rather than from the outer surface of C_3S . This C-S-H being on the outer surface is called as “outer C-S-H”. After 18 hours of hydration, longer ettringite rods are formed when C_3A reacts with more gypsum. Network of C-S-H and longer ettringite rods form a “hydrating shell” at an approximate distance of $1\ \mu\text{m}$ from C_3S surface particles. In later stages, “Inner C-S-H” is formed in this hydrating shell. After 1–3 days of hydration period, deceleratory period kicks in due to a slowdown in reactions. During this stage, C_3A reacts with longer ettringite rods to form mono-sulfate. Narrowing the gap between “hydrating shell” and C_3S surface, inner C-S-H continues to grow on the outer surface of C_3S particles. Based on the diffusion rate of ions or water to the anhydrous C_3S surface, rate of hydration changes. After 2 weeks of hydration, “inner C-S-H” occupies the gap between the hydrating shell and $1\ \mu\text{m}$ space gets completely filled with C-S-H. Meanwhile the “outer C-S-H” grows in length and becomes more fibrous in length [10]. Fig 2.2 represents the hydration process of anhydrous cement.

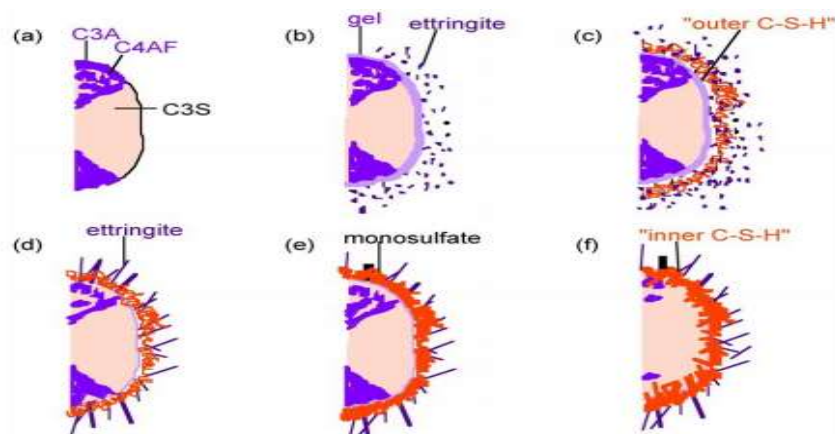


Fig 2.2: Figure representing the hydration process in cement (a) before hydration (b) 10 minutes, (c) 10 hours, (d) 18 hours, (e) 1–3 days, and (f) 2 weeks. [10]

2. Structural Analogues of C-S-H

There are at least thirty crystalline minerals [11] that could resemble the composition of C-S-H gel. According to the TEM [12] and XRD investigations [13], C-S-H gel exhibits layered features of the tobermorite [14] and jennite structure [15].

Tobermorite:

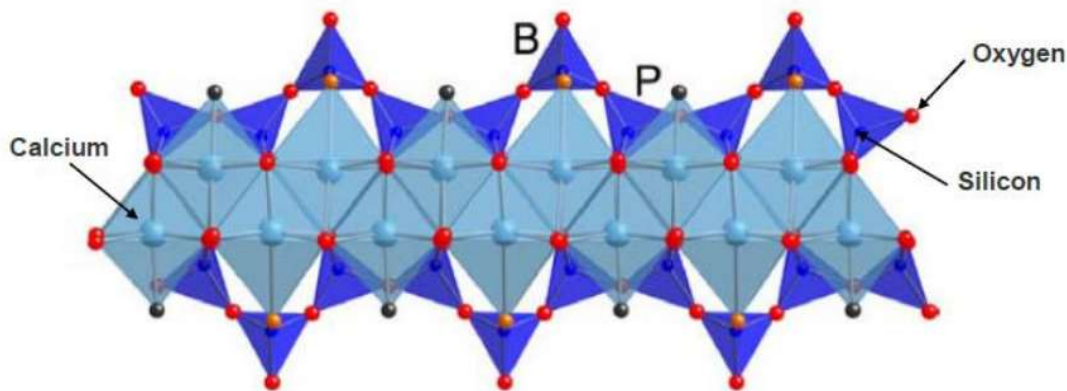


Fig 2.3: C-S-H layer showing a main calcium octahedral layer with silicate tetrahedron attached on both sides. Calcium octahedral, Silicate chains and oxygen atoms are shown as light blue, dark blue tetrahedron, and red spheres respectively. P-pairing, B-bridging tetrahedrons [14]

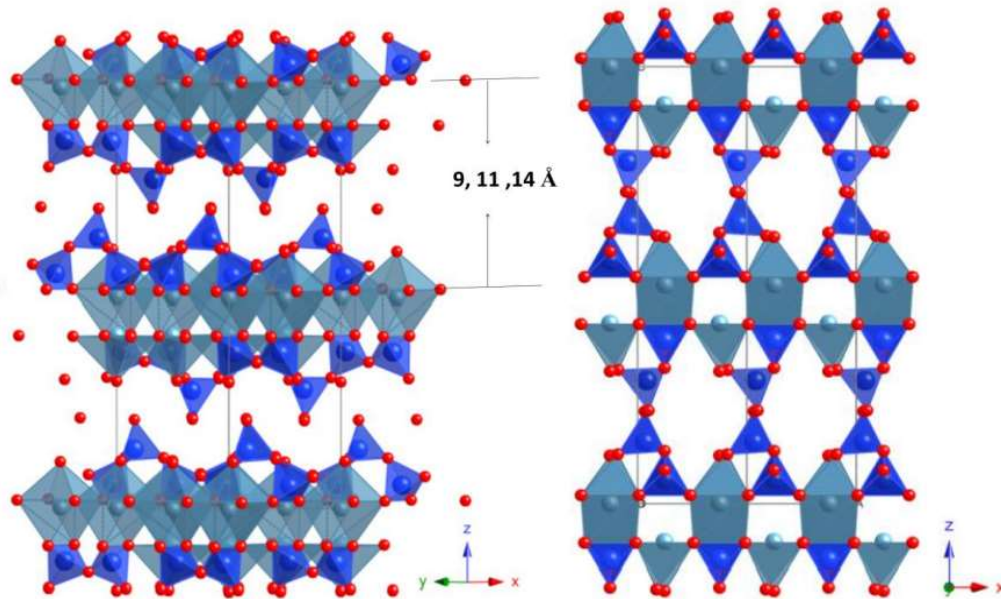


Fig 2.4: Crystal Structure of Tobermorite 11 Å proposed by Hamid. Calcium octahedral, Silicate chains and oxygen atoms are shown as light blue, dark blue tetrahedron, and red spheres respectively [14]

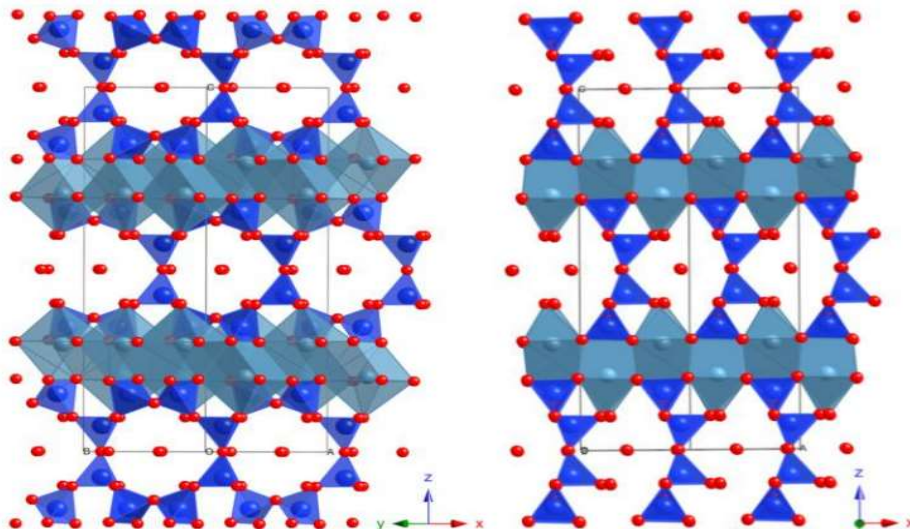


Fig 2.5: Crystal Structure of Tobermorite proposed by Merlino [16]. Silicate chains, calcium octahedral, and oxygen atoms are shown as dark blue, light blue tetrahedron, and red spheres, respectively.

Tobermorite is a calcium silicate hydrate mineral that exists in nature. Three different types of tobermorite exist, i.e., 14 Å, 11 Å or 9 Å tobermorite. They are distinguished based on the different basal spacing corresponding to different hydration degree [17]. The 11 Å tobermorite has a layer structure and consists of a central sheet of calcium with silicate chains sandwiched as shown in Fig 2.3. The so-called Dreierketten chains as shown in Fig 2.3 that two “paired” tetrahedrons point towards Ca sheet and one “bridging” tetrahedron linked with interlayer form a basic unit (period) for repetition. The nearest silicate chains are not aligned “head to head” but rather shifted by some amount. Calcium atoms and water molecules are present between two layers of calcium-silica sheets. As confirmed by the NMR measurements, the Q^2 silicate sites are dominant, implying the infinite length of the silicate chain.

Additionally, tobermorite 11 Å has two different structures: Hamid structure which is a refinement that describes the tobermorite as independent layers [14] and

Merlino structure which considers tobermorite as chemically bonded layers [16]. The major difference between Hamid shown in Fig 2.4 and Merlino structures shown in Fig 2.5 is the interlayer connection between the bridging tetrahedrons. As shown figures the head-to-head connection of bridging tetrahedrons forms an ionic-covalent Si-O-Si bond with the neighboring calcium silicate sheets. While Q² species change to Q³ species, the 2D single silicate chains transforms to the 3D branch and network. Furthermore, thermal behavior of tobermorite investigated by multiple experimental techniques indicates the transformation from tobermorite 14 Å to 9 Å: tobermorite 14Å transforms into tobermorite 11 Å by heating up to 80°C~100°C and further heating up to 300°C for transformation to 9 Å.

Jennite:

Jennite is a natural and rare silicate mineral that has been found in several regions in the world such as Israel, Germany and Japan. Based on the data collected on a thin crystal using X-ray diffraction data, Bonaccorsi et. al. solved the crystal structure of Jennite[15]. The solved crystal structure of jennite is shown in Fig 2.6, in two different projections. The structure consists of three ribbons: ribbons of edge-sharing calcium octahedral, wollastonite-type silicate chains, and a calcium octahedron on inversion centers. These ribbons connected with each other gives a zigzag layered structure to calcium octahedron. Silicate chains help to firmly link these distinct ribbons. From the analysis of hydrogen bonds connecting the H₂O molecules, it is concluded that both oxygen and hydroxyl anions co-exist in jennite. The chemical formula of jennite is Ca₉Si₆O₁₈(OH)₆·8H₂O. The Ca/Si ratio in jennite

reaches 1.5, a value greater than that in tobermorite and much closer to the mean Ca/Si ratio of the hydrated cement.

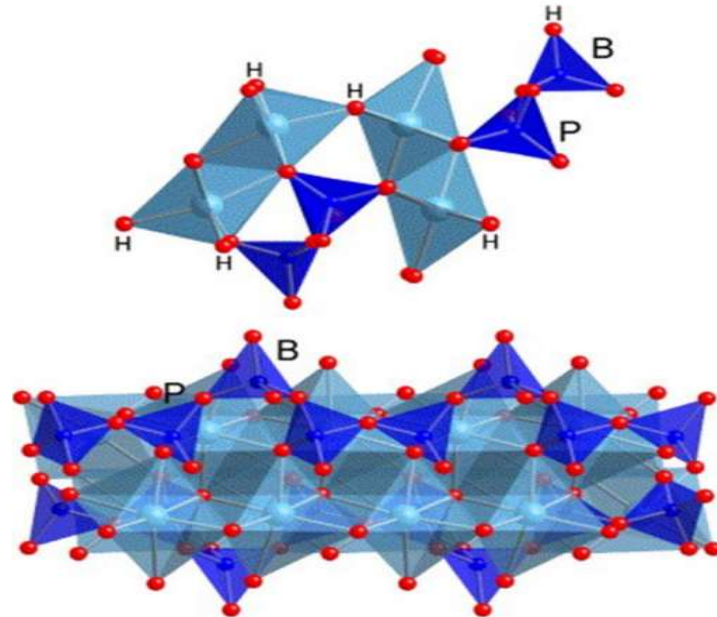


Fig 2.6: Crystal Structure of jennite projected along [010] (top) and [100] (bottom). Calcium octahedral, Silicate chains and oxygen atoms are shown as light blue, dark blue tetrahedron, and red spheres respectively. P-pairing, B-bridging tetrahedrons, H-hydroxyl group [15].

3. Morphology and Layered Feature of C-S-H

From the hydration process, at micro-meter scale, the morphologies of C-S-H gel can be categorized into two types: inner products (IP) and outer products (OP). IP is also referred as HD phase, OP is referred as LD phase based on density. The IP grows near the cement grains and has relative high density. It is composed of aggregated globule particles of 4nm-6nm and the pore size inside the IP is less than 10nm. On contrary, for the OP, less space restriction and sufficient water environment can make the structure grow to fibril-like (length to width ratio is high)

morphologies. This kind of structure can leave large porosity between the fibrils. TEM micrographs of IP and OP C-S-H is shown in Fig 2.7.

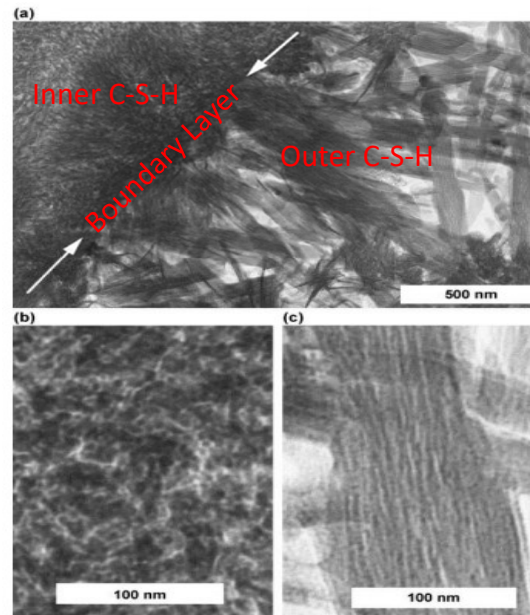


Fig 2.7: (a) TEM micrograph showing inner and outer C-S-H in a hardened C_3S paste. White arrows shows the boundary layer (b) globules of inner C-S-H. (c) fibrillary structure of outer C-S-H. [12]

At meso-scale, less than 1 μm , Atomic Force Microscopy (AFM) can help characterize C-S-H. From AFM photos [18] shown in Fig 2.8, the boundaries between ellipsoid shaped C-S-H particles and the packing orientation of those particles can be observed. Furthermore, recent series of nano-indentation tests prove the granular mechanical properties of C-S-H particles [19] and Small Angle Neutron Scattering (SANS) tests also indicate the existence of nano-particles aggregation. These nanoparticles are called as basic building units of C-S-H [20]. Nevertheless, the shapes, sizes and packing distribution for the C-S-H particles are not determined quantitatively. The formation mechanism of the C-S-H colloid is still under debate.

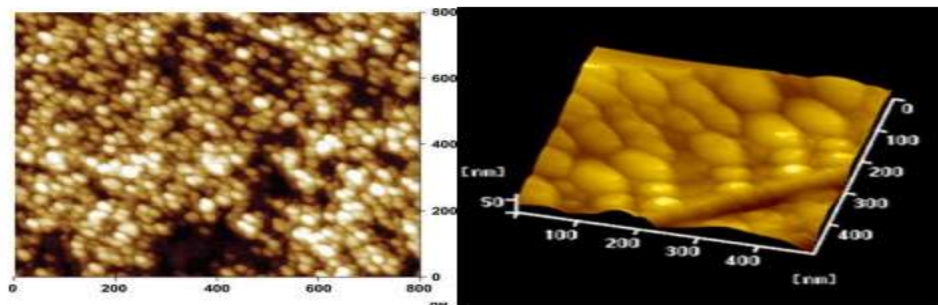


Fig 2.8: AFM photos of C-S-H particles on a nanoscale. [18]

At the nano-meter level, multiple techniques such as AFM, NMR, SANS, Small Angle X-ray Spectroscopy (SAXS), Dark Field TEM(DFTEM) have been attempted to probe the molecular structure of C-S-H. Nevertheless, these methods cannot observe the structure in a straightforward manner and no consistent model has been proposed using a single testing technique.

Layered Feature:

X-ray diffraction is a very powerful tool to investigate and understand the structure of nano-crystalline C-S-H. Previous XRD results of C-S-H with Ca/Si ratios varying from 0.6 to 1.7 are in accordance with nano-crystalline and turbo-stratic tobermorite that is a layered calcium silicate crystal [14]. By studying the synthesized C-S-H gel, XRD patterns shows the diffraction maxima at 7.4° (12.0 \AA), 16.7° (5.3 \AA), 29.1° (3.1 \AA), 32.0° (2.8 \AA), 49.8° (1.8 \AA), 55.0° (1.7 \AA) and 66.8° (1.4 \AA). The maxima observed are mostly asymmetric and broad, the maxima at 7.4° (12.0 \AA) shifts in position and intensity with change in Ca/Si ratio of C-S-H [21] [22]. XRD intensity file from [21] for example shown in Fig 2.9, the patterns are similar to those obtained for poorly crystalline tobermorite of 14 \AA , with broad basal reflections in the d-range

of 20–10 Å and further reflections at 5.30, 3.07 (strongest), 2.80, 1.83, 1.67, 1.53, 1.40, 1.19, 1.11, and 1.07 Å. From the XRD patterns it can be said that C-S-H is a layered structure. However, when compared with other layered structures, line broadening in the spectra can be attributed to nano size of crystal, whereas asymmetry is can be attributed to turbo-stratic disorder. Turbo-stratic disorder is defined as random translations parallel to layers occurring between successive layers in a systematic manner.

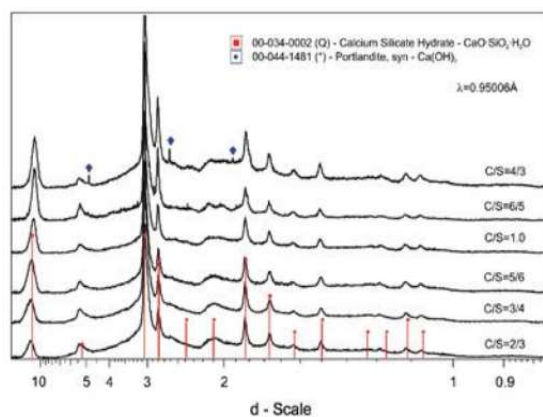


Fig 2.9: X-ray diffraction (XRD) patterns of nano-crystalline C-S-H phases with different Ca/Si ratios. Wavelength=0.95006 Å [21]

Regarding the defective layered features of the C-S-H gel, the layered order cannot persist in long range. It can be observed from that compared with true tobermorite, the crystal length is dramatically reduced and the layered orientation is disturbed. The results are evident from Fig 2.10.

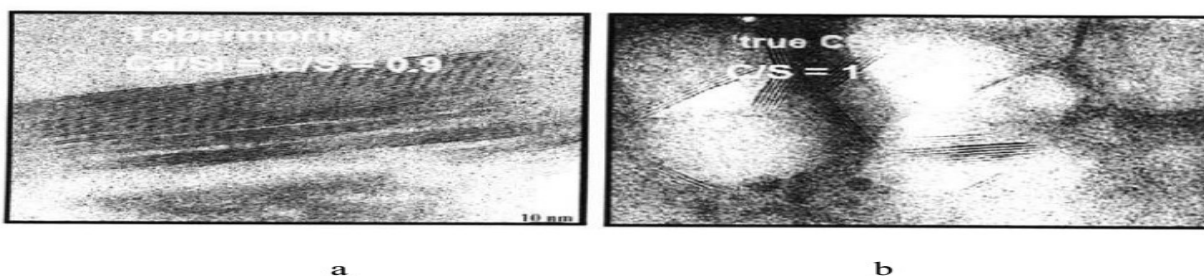


Fig 2.10: TEM photos for the tobermorite and C-S-H. a: A synthesized C-S-H with Ca/Si=0.9, quite similar to the tobermorite structure. b: C-S-H gel with Ca/Si=1.7 [13]

4. Density and Water Content in C-S-H

The density of the C-S-H gel is closely related with the water content in the gel pores. From water pycnometry, the density of dried C-S-H was found to be at 2.85 Mg/m³ [23]. Recently, scattering techniques such as X-ray and neutron have been used to determine the density and water content of C-S-H globules with great accuracy [20]. Chemical formula of C-S-H is C_{1.7}SH_{1.8} and its density is found to be at 2.604 Mg/m³. This density includes both evaporable and non-evaporable water present within the saturated C-S-H globules, but do not include water present on outside of the globules or water adsorbed on the surface. ¹H NMR helps to characterize the nano-porosity of C-S-H without damaging the drying process of the sample. The density of C-S-H changes as a function of water to cement ration and degree of hydration (α). Density evolution of the C-S-H gel has been detected by the NMR technique. The “solid” C-S-H density, excluding water present in between gel pores, decreases slightly from $\rho = 2.73 \text{ g/cm}^3$ at $\alpha \approx 0.4$ to 2.65 g/cm^3 at $\alpha \approx 0.9$, this change can be attributed to increase in number of layers in the nano-crystalline globules. The “bulk” density of C-S-H, including water in between the gel pores, increases from 1.8 to 2.1 g/cm³.

Jennings [24] summarized the density evolution of the C-S-H at different water states. With removal of evaporable water, a single sheet of C-S-H has a density of 2.88 g/cm³. A fully saturated globule of C-S-H without adsorbed water on the surface reduces the density to 2.602 g/cm³. Fig 2.11(A) represents a fully saturated C-S-H globule with a single layer of water on the surface and both Intra Globular Pores

(IGP) and interlayer pores full representing 11% relative humidity. Fig 2.11(B) represents partially dried C-S-H layer with much of the interlayer and monolayer water removed.

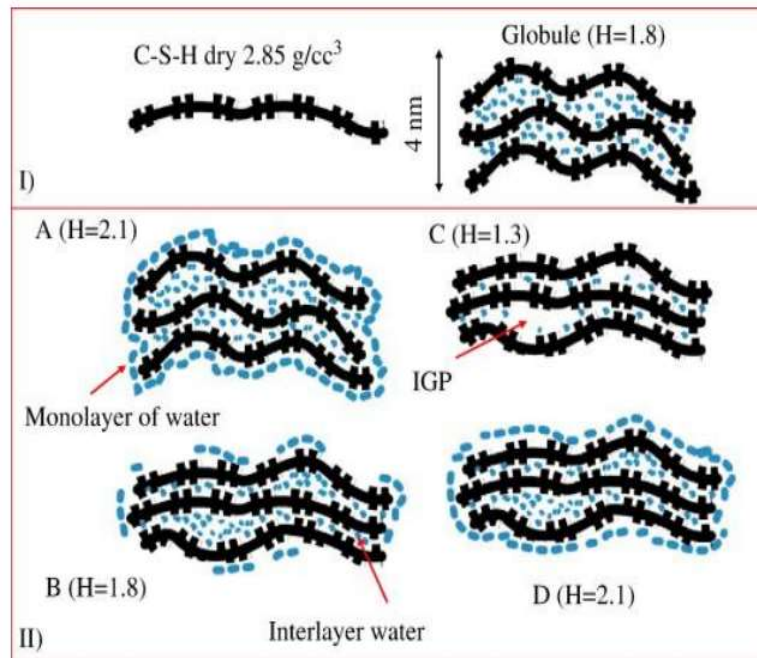


Fig 2.11: Figure representing C-S-H globule with representing change in water content states obtained during drying from 11% RH and rewetting to different RH and again returning to 11% RH [24]

There is a decrease in volume of globule with monolayer of water, density increased from that of fully saturated C-S-H globule. In order to represent the d-dried state, all evaporable water is removed. Density decreases due to the presence of empty IGP. By rewetting, IGP are filled with water and also monolayer comes back around the globule.

5. MODELS OF C-S-H

Several micro-structural models have been proposed to describe the micro-structure of C-S-H gel at nano-scale and formation of gel pores during the past few

decades. Of the models, three models, proposed by Powers and Brownyard, Wittmann, and Jennings and Tennis, have been used widely. Powers and Brownyard model and Jennings model are discussed below.

Powers and Brownyard model:

Powers and Brownyard [25] proposed a model for the structure of cement gel based on their studies of water vapor sorption isotherms and water chemically bound in hardened cement pastes. In their model, the C-S-H gel is made of particles with a layered structure, which are composed of 2-3 sheets. As shown in Fig 2.12, the randomly distributed layers are bonded together by linking adjacent particles with strong ionic-covalent surface forces.

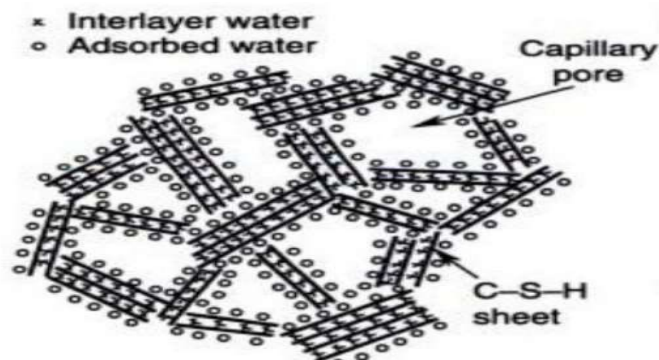


Fig 2.12: Powers and Brownyard model [25]

Based on their studies, water molecules in the C-S-H gel are of three types: water of constitution, capillary water and gel water. Water of constitution involves water that helps in crystallization, non-evaporable and chemically bound water, including the hydroxyl groups associated with metallic ions Ca-OH. Gel water includes adsorbed water and water bound by physical surface forces. These water

molecules are packed between the layers of the crystal hydrate. On the other hand, the capillary water is free water inside the pores, not bound by the surface force.

Jennings model:

This model is one of the widely accepted in present days. Compared with previous models, Jennings model gives a comprehensive description for the C-S-H gel in the respects of the surface area, density and water content [26] [24]. In this model, Jennings proposed that the C-S-H gels are aggregation of the colloids with nano size. The smallest building blocks are colloid spheres with diameter 2.2nm and density 2.8g/cm³. From Fig 2.13, agglomeration of these spheres can form larger globules with diameter 5.6nm.

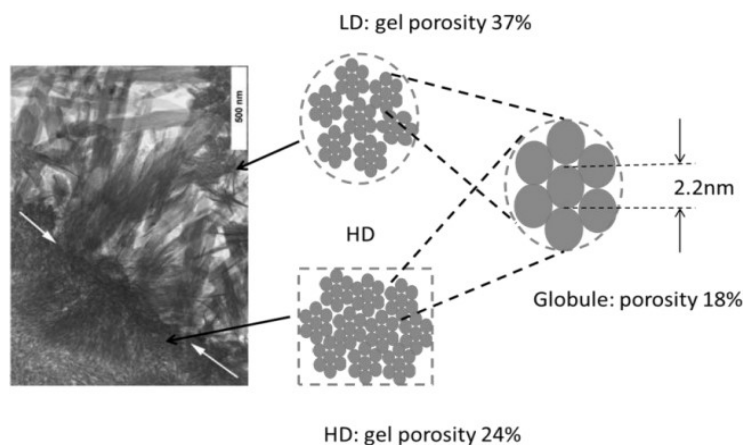


Fig 2.13: Jennings colloidal model [26]

Those globules aggregated together according to different packing efficiency can result in two main species of the C-S-H gels: high density (HD) with 24% porosity and low density (LD) with 37% porosity. The HD and LD phases of C-S-H gels can explain the morphologies of dense IP and loose OP respectively. This can help interpret the contradictory results of surface area from multi techniques. For

example, even though the HD phase occupies large surface area/volume, the N_2 cannot penetrate into the narrow pores in HD phases. This colloidal model proposed by Jennings explains several properties of C-S-H present in cement paste. The main basis of this model is that C-S-H is made of building blocks of size $<5\text{nm}$. Although several experiments such as electron microscopy, neutron scattering and molecular simulations suggested the presence of nano grains, existence of such particles is yet to be proved.

Atomic Models of C-S-H:

The molecular structure of the C-S-H gel has been investigated by many researchers in the physics and chemistry fields. The C-S-H gel is characterized by the layered features, tobermorite analogues and silicate chains distribution that are predicted from many experiments such as the XRD, NMR and TEM [27] [12] [28].

Taylor and Howison [29] suggested that the Ca/Si ratio of 0.8 in Tobermorite could be increased by omitting the bridging silicate tetrahedrons and replacing them by calcium atoms. Some other studies proposed that Jennite has a structure closer to C-S-H. Half of the oxygen atoms in Jennite present in the central calcium sheet of the C-S-H layer are shared with hydroxyl(OH^-) groups. But in tobermorite, infinite parallel silicate chain rows share the oxygen atoms.

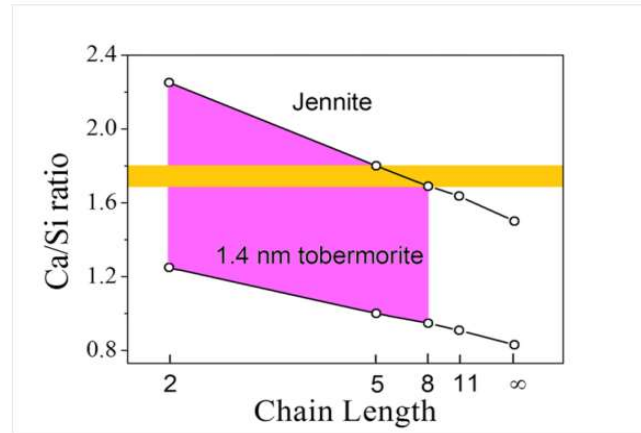


Fig 2.14: Relationship between Ca/Si and silicate chain length of tobermorite and jennite based on tobermorite and jennite structures [30]

Taylor proposed that C-S-H structure is a mixture of crystal structures of jennite and tobermorite and C-S-H is a disordered layer structure. Fig 2.1 shows one of the theoretically possible ways to explain the high Ca/Si ratio of C-S-H (1.7 to 2.0). Dimeric 1.4nm tobermorite and jennite have a Ca/Si ratio of approximately 1.25 and 2.25 respectively during the early stages of development. Since the study of Taylor, there has been a general agreement that C-S-H with $\text{Ca/Si} < 1$ is a disordered layer structure of 1.4 nm tobermorite.

Model Based on Molecular Simulation:

Even though the modified tobermorite and jennite models discussed above demonstrate some similarity with the C-S-H gel, these C-S-H analogues do not possess strict structural and morphological resemblance to those in realistic C-S-H. These theoretical models have not comprehensively considered the basic physical properties such as the density, Ca/Si ratios, silicate chain distribution and water content, and so on

Based on the chemical composition of C-S-H as the essential properties, the “realistic model” of C-S-H gel was constructed by the assistance of the molecular simulation [31]. The consistent molecular model, systematically considering the properties of C-S-H gel acquired from multiple experiments, has demonstrated the interaction between CaO, SiO₂ and H₂O to form a defected silica chain morphology that links to realistic values for density and chemical composition of an averaged C-S-H phase. As shown in Fig 2.15, the chemical composition of C-S-H model, (CaO)_{1.65}(SiO₂) (H₂O)_{1.75}, suggests that the C-S-H structure has both tobermorite like crystalline features and glass like short-range order. Validated by experiments, the model also predicts several essential structural features and fundamental properties such as stiffness and strength of a real cement paste system. The realistic model is the first attempt in understanding the cement structure at nano-meter scale by molecular simulation. However, the model proposed by Pellenq still has some limitation: the silicate chain backbone, hydroxyl groups and the local structure of calcium octahedron should be further improved to accurately describe the C-S-H molecular structure. Also chemical composition, including water contents and Ca/Si ratio has not been considered sufficiently in the proposed model. From this model it was found that during the middle period (4-24 h) structure of C-S-H is dynamic, changing rapidly with time filling pores and flocculating basic building blocks forming the micro-structure. This is the period when LD C-S-H is formed. From SANS experiments it was observed that the basic building units are jammed together without change in the internal structure thereby forming globules.

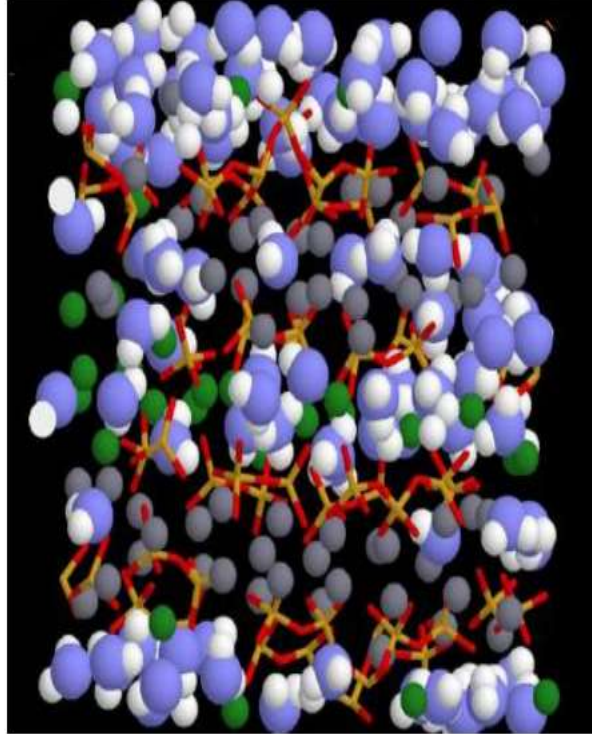


Fig 2.15: Realistic molecular model of C-S-H. White and blue spheres are hydrogen and oxygen atoms of water molecules respectively. Gray and green spheres represents intra and inter-layer calcium ions respectively. Red and yellow sticks represents oxygen and silicon atoms [31]

From SANS experiments it was observed that the basic building units are jammed together without change in the internal structure thereby forming globules. This model also shows that, a packing efficiency of 82% is achieved when the basic building units are packed together into a 3D structure. If the packing can be controlled during this dynamic stage, cement can be engineered to form denser packing leading to high strength final product.

CHAPTER III

SCANNING ELECTRON MICROSCOPY

1. Introduction

SEM is used for sample surface investigation. Surface topography of the sample is observed by 2D scanning of the electron probe over the sample surface and image can be obtained from the secondary electrons(SE) detected [32]. SEM consists of an electron optical system in order to produce an electron probe, a sample stage surrounded by vacuum to place the sample, a secondary electron detector in order to detect secondary electrons and an image display unit. The electron optical system comprises of an electron gun, an objective lens to produce electron probe and a condenser lens. When the electrons from an electron gun hits the sample surface, various electrons and electromagnetic waves are emitted from the sample surface. Secondary electrons emitted from the surface are detected by secondary electron detector. These output signals from SE detector are amplified and then transferred to the display unit [32]. Since the display unit is in sync with the electron probe scan, variation in brightness, which depends on the number of secondary electrons detected, appears on the display unit forming a SEM image. SEM and EDS were used to find out the C-S-H phases in a composite sample as the hydrated sample has different other phases present.

2. Sample Preparation

Proper specimen preparation is important for SEM study of cement and cementitious materials. Rough sample surfaces prepared using saw-cut, fracture or

uneven-lapped preparations doesn't give good representative images. Improper sample preparation for SEM introduces artifacts that doesn't represent the microstructure. They also create an uneven surface unsuitable for phase abundance estimation. X-ray and backscattered imaging are very sensitive to rough surfaces affecting the constituents due to signal shadowing and contrast loss.

For SEM analysis, cement paste with water-cement ratio of 0.13 was used. Cement paste was prepared using ordinary Portland cement and tap water to mimic field conditions. Then, the paste was stored in closed recipients (film canisters) which act as molds. Samples were cured in a temperature controlled curing room at 24°C. Samples were removed from the curing room at different time points of 18 hours, 1 day, 2 days, 3 days, 4 days, 5 days, 6 days and 7 days so that hydration can be stopped at different hydration times.

Drying Techniques:

Free water was removed from hydrated cement samples using solvent exchange method and oven drying. For the solvent exchange method, cement samples removed from the curing room were placed in containers filled with 200 proof Ethyl alcohol to remove any free water present in the sample [33]. Before epoxy impregnation, to remove any alcohol or water remaining in the pores, samples were oven dried at a 105°C in atmosphere without controlling humidity for 24 hours. Samples were always stored in desiccator with silica gel to keep them free of moisture and CO₂.

Epoxy Impregnation:

Epoxy impregnation is mainly used to serve two purposes: 1) To fill the voids and support the microstructure against cracking due to shrinkage upon curing, 2) To enhance contrast between pores, hydration products and cementitious materials [34]. An ultra-low viscous epoxy was used to help rapid infiltration of the pore structure. A section of the material was sawn and dried at a temperature 65°C. Water is removed so that there is no interference with polymerization of epoxy. The sample is put in a container filled with epoxy. The top is open to fresh air allowing microstructure to be filled with epoxy by capillary action. The epoxy is then cured for 24 hours under low temperatures. Epoxy impregnation also helps in mounting the samples onto SEM sample stubs.

Cutting:

The most important requirement for SEM analysis is to cut the sample to size. Cutting, grinding and polishing were done to expose a fresh surface of the specimen. Cutting is generally done using saw or cutting wheel. When a regular saw or cutting wheel is used, surface gets damaged occurs and the damage can extend up to $200\mu\text{m}$ or more into the sample. Therefore, fine cutting tools should be used for SEM analysis [34]. A 5" lapidary diamond trim saw with a diamond impregnated wheel was used for cutting the epoxy impregnated sample. These wheels have counter balanced loading which avoids excessive pressure on the cutting specimen. Ethyl alcohol was used as a lubricating agent to prevent the entry of water into the micro-structure of cement sample. Samples were cut into 1" diameter with a thickness of $1/32"$.

Grinding and Polishing:

After the sample was cut, in order to get uniform image across the cross section, cut surface needs to be ground and polished. The epoxy mold helps to hold the specimen during grinding/polishing. Grinding was done using Apex 8" 45 μ m diamond grinding disc from Buehler using manual grinding. The sample was rotated in a figure 8 or circles and by alternating grinding direction by 90⁰ for effective grinding. Visual examination of the sample surface allows for the identification of when the entire surface has been grinded. Grinding striations on the sample surface helps to identify that the grit had completely removed a layer of material. 200 proof ethyl alcohol was used as a lubricating agent to avoid entry of water into the specimen.

Polishing helps in removing damage to the sample surface introduced by the sawing and grinding. Diamond polishing pastes with a particle size ranging from 6 μ m to 0.25 μ m are used in a successive sequence. A lap wheel covered with a low-relief polishing cloth is used for polishing. Polishing was done on a semi-automatic polishing machine using mono-crystalline diamond suspensions of sizes 9 μ m, 3 μ m, 1 μ m and an alumina micro polish of 0.05 μ m for final polishing. 2-7/8" Trident polish cloths were used for polishing the samples using diamond suspensions and a micro cloth was used for final polishing with alumina. Table 1 represents the polishing procedure used for these samples.

Surface	Abrasive/size	Load lb./Specimen	Base Speed(RPM)	Relative Rotation	Time(min:s)
Trident polish cloth	9 μ m diamond oil based suspension	5	120-180	>>	5:00

Trident polish cloth	3 um diamond oil based suspension	5	120-180	>>	4:00
Trident polish cloth	1um diamond oil based suspension	5	120-180	>>	4:00
Micro cloth	0.05 um micro polish alumina with ethyl alcohol	4	100-150	><	2:00
<p>*>> = Polishing plate and sample holder rotate in same direction >< = Polishing platen and sample holder rotate in opposite direction</p>					

Table 1: Concrete bulk mount preparation method with diamond suspensions

Coating and Conductivity:

During SEM imaging, non-conductive samples can absorb the electrons, accumulating negative charge thereby repelling the electron beam and degrading the image [34]. In order to avoid this, specimens are coated with a thin conducting film. Carbon is the common coating material which is cheap and almost invisible to X-rays. If the sample surface is irregular, Gold or gold-palladium is used as a coating material and if there is no need for compositional analysis or else it will interfere with the peaks in spectrum. The most common techniques used are thermal evaporation and sputter coating. Carbon sputter coating was used to coat the polished samples. Modern low voltage sputters enable metal to be deposited at 1nm/s in a low vacuum environment. Coating was done at Nanomaterials Characterization Facility (NCF), University of Colorado Boulder. A thin carbon layer of 15nm was coated on all the sample surfaces. Fig 3.1 shows the final samples after polishing and the carbon sputter coating machine.



(a) (b)
Fig 3.1: a) carbon sputter, b) samples mounted on sample stub

3. SEM Imaging Procedure

All SEM and EDS was done at NCF, University of Colorado Boulder using a JEOL JSM-6480 LV SEM. Fig 3.2 shows the SEM machine setup at NCF. Before starting with SEM imaging, to avoid outgas, samples must be completely dry and clean. Dirt particles were removed by blowing compressed gas on the sample surface. 1" diameter cylindrical sample stubs were used to mount the specimens. A double coated conductive carbon tape was used to hold the specimen firmly on the sample stub so that it will not move during the imaging. The vacuum chamber in the SEM machine must be vented with air before placing the sample stub in the chamber. After the chamber is vented, the sample stub was mounted onto the sample stage in the chamber. Gloves were used so that vacuum chamber stays free of any impurities which may damage the apparatus. The door to the vacuum chamber was closed and the chamber was evacuated to create vacuum. The sample stage was moved such that the electron detector is close to the top surface of the sample but not too close. An infrared (IR) camera was used to see that the sample surface and the detector are at a safe operational distance. Now, the electron beam is turned on to image the sample surface.

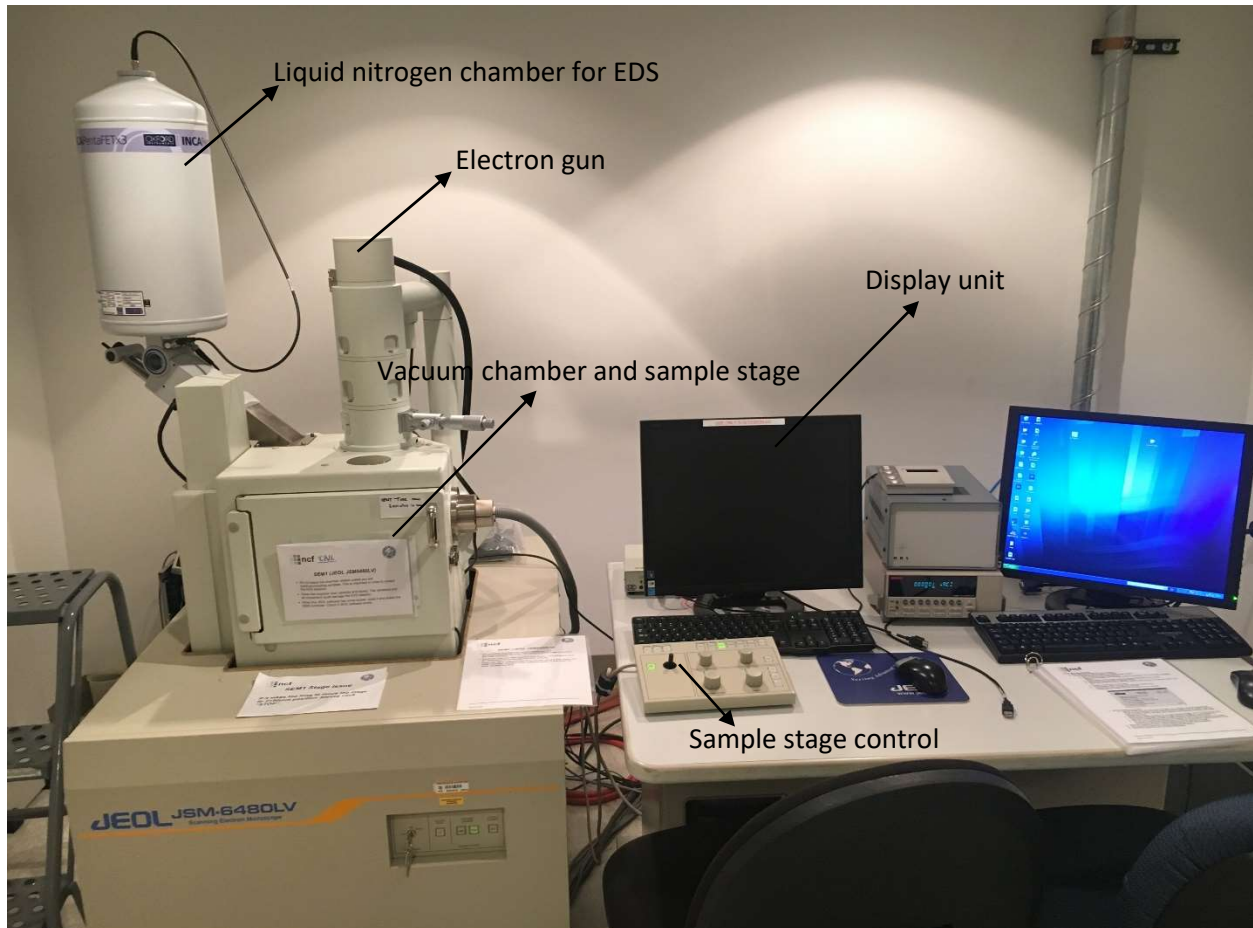


Fig 3.2: JEOL JSM-6480 LV SEM machine at NCF

Using different operational settings, a clear and high resolution images were obtained at an accelerating voltage of 15-20Kev, spot size of 65-69, working distance 8-10mm and using secondary electron(SE) signal. The objective lens was moved along the surface of the sample and imaging was done at desired locations at length scales of 100 μ m, 10 μ m, and 1 μ m. The same process was repeated for all the samples stopped at different hydration times of 18 hours, 1 day, 2 days, 3 days, 4 days, 5 days, 7 days.

4. Results

For early hydration stop samples, a length scale of 100 μ m had a good resolution and clear representation of growth of the cement matrix. For later hydration times,

clear pictures were obtained on a length scale of 10 μ m. 1 μ m images were not clear as the SEM machine highest resolution is 1 μ m. Figure 3.3 represents the evolution of cement matrix with hydration time. Evolution on different length scales of 1 μ m, 10 μ m and 100 μ m are shown.

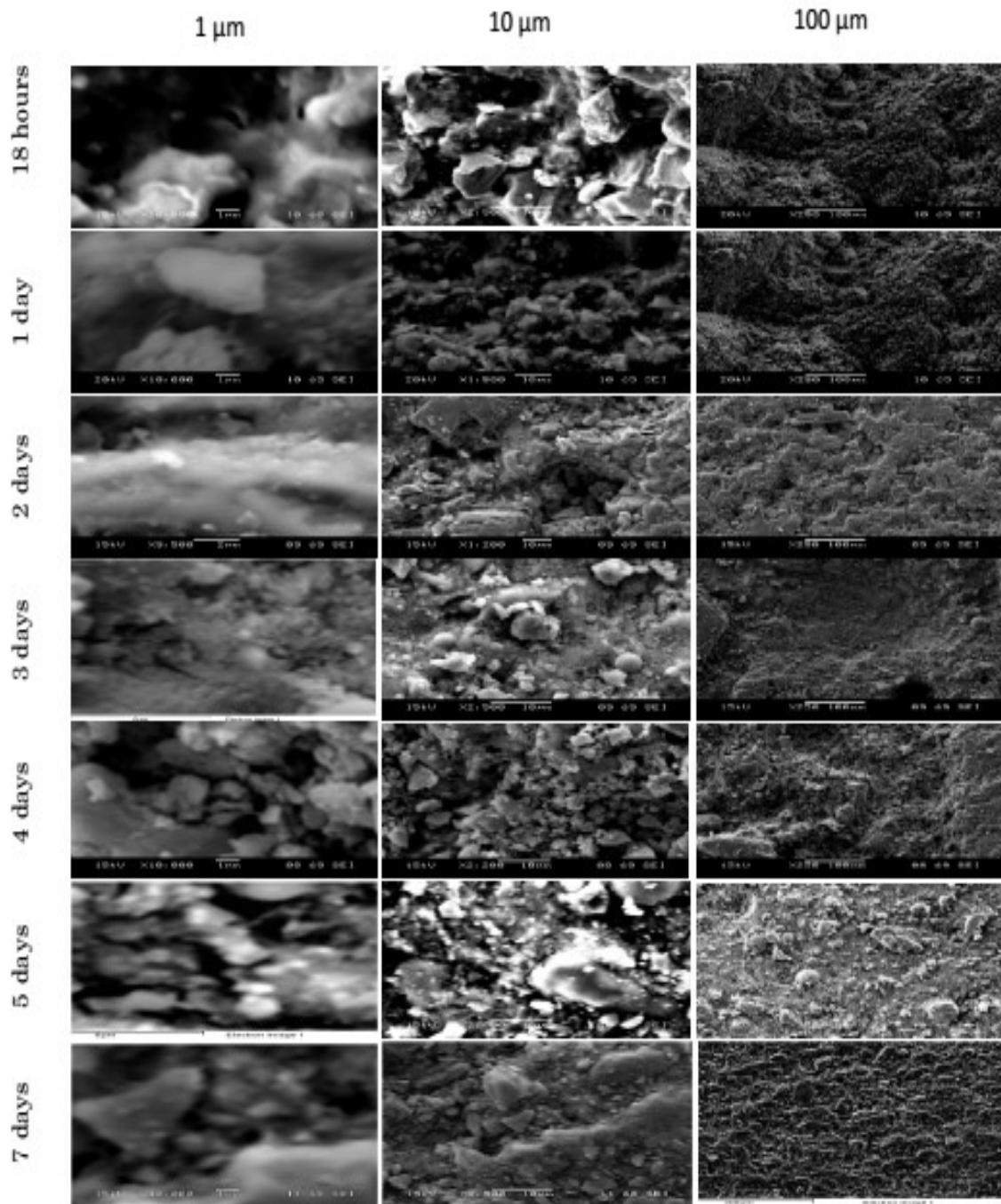


Fig 3.3: SEM image showing evolution of cement matrix with hydration time.

5. Discussion

SEM analysis was done to obtain preliminary evolution images for different hydration time. It can be seen from the 10 μ m images, the cement matrix evolved from smooth globules to textured fibrillary material. This represents the growth of C-S-H in cement matrix. EDS was done on these samples to find out exactly where the C-S-H phase is present in the sample which is discussed more in next chapter. SEM imaging gives a visual representation of how the sample surface looks and it is difficult to draw discernable conclusions from the images.

CHAPTER IV

ENERGY DISPERSIVE SPECTROSCOPY

1. Introduction

EDS when combined with SEM imaging can provide spatially resolved elemental analysis from areas as small as 1nm in diameter. Due to presence of elements with different atomic numbers and different distributions, backscattered electron images have compositional contrast. When electron beam hits the sample surface, EDS detects the back scattered electrons emitted and gives the elemental composition of the analyzed area [35]. Electrons are ejected when an electron beam hits the sample surface, these electron vacancies when filled with higher state electrons emits an x-ray to balance the difference between the two energy states. Each element has x-ray of characteristic energy. Using these characteristic energies, EDS detects the presence of elements in a scan area.

Relative abundance of x-rays emitted versus their energy is measured by the EDS detector. A charge pulse proportional to the energy of x-ray is created when an x-ray hits the EDS detector. From the charge pulse, the energy for each incident x-ray is sent to the computer for data evaluation and display. Data evaluation gives a spectrum which is evaluated to determine the elements present in the sampled volume. The y-axis represents counts, which is number of x-rays received and processed by the detector and the x-axis represents the different energy level of the counts. Three different kinds of spectra are obtained in this study: spot spectrum, areal spectrum, and line spectrum. Also, a smart map of different elements present in the sample was obtained using the smart mapping option in the analysis software.

Spot Spectrum:

When the electron beam is kept stationary at a spot or a series of spots, spot spectra is generated which provides more localized elemental information on the sample. The SEM image shows where the spots were selected for the corresponding spot spectrum. All the spots were selected randomly on the specimen. Spots were selected on a smooth surface to give a good elemental representation of the sample.

Areal Spectrum:

When the electron beam is focused on an area rather than a point, areal spectrum is obtained. The SEM image shows the area selected for the corresponding areal spectrum. The areal spectrum gives an overall elemental representation of the area selected.

Line Spectrum:

Line spectrum is generated when the sample surface irradiated with an electron beam across a line. Emitted x-rays are detected for different positions along the line by EDS detector. Spectrum is produced along the length of the line, providing relative elemental composition for each element along the line length.

2. EDS Experimental Procedure

All the samples with different hydration times were analyzed for EDS. There was no separate sample preparation for EDS as samples prepared for SEM can be used for EDS also as long as they are well coated with carbon. JEOL JSM 6480-LV as shown in Fig 3.2 was used for EDS. Once a clear SEM image was obtained using secondary electron detector, EDS was done on the same images to obtain the spectra

for different locations. The Backscatter electron (BE) detector was used to obtain the spectra. The SEM machine at NCF uses INCA analysis platform by Oxford Instruments to obtain different types of EDS spectra and smart maps of the sample. The coating material, thickness and density was input into the INCA software so that carbon peak due to coating is omitted out of the spectra representing the true composition of the sample. The accelerating voltage must be greater than 10kV to obtain EDS spectra. After obtaining the SEM image, based on the type of spectra (spot, areal and line), the target area on the specimen was selected to obtain the spectra. AutoID in INCA detects the elements based on the energy peaks in spectrum and their corresponding characteristic energy value. After the spectrum is obtained, the confirm elements option in INCA provides tools to manually validate the elements detected. Some spectra showed peaks with elements which were not in the sample and confirm elements option was used to manually validate the elements. Elements were quantified automatically based on the elements identified to represent the relative abundance of elements in analysis area. Quantitative analysis gives weight% and atomic weight% in the target area. A smart map was obtained to find the distribution of different elements on the sample surface. A report with all the images and spectra was generated for each sample.

3. Results

Results from EDS analysis for each sample with different hydration stop times were obtained. Each sample has an electron image and corresponding EDS spectrum. Each peak in the spectrum denotes the presence of the element in the total scan area

of the image. Line spectrum and spot spectrum are not shown in the results as all the spectrums are almost the same. Smart maps of only three elements: Oxygen(O), Silica(Si), Calcium(Ca) are shown for each sample as they are the main constituents of C-S-H. Fig 4.1 represents EDS spectra and smart map for the 18 hours sample with phases identified on them. EDS spectra and smart maps for samples from 1 day-7 days are shown in appendix.

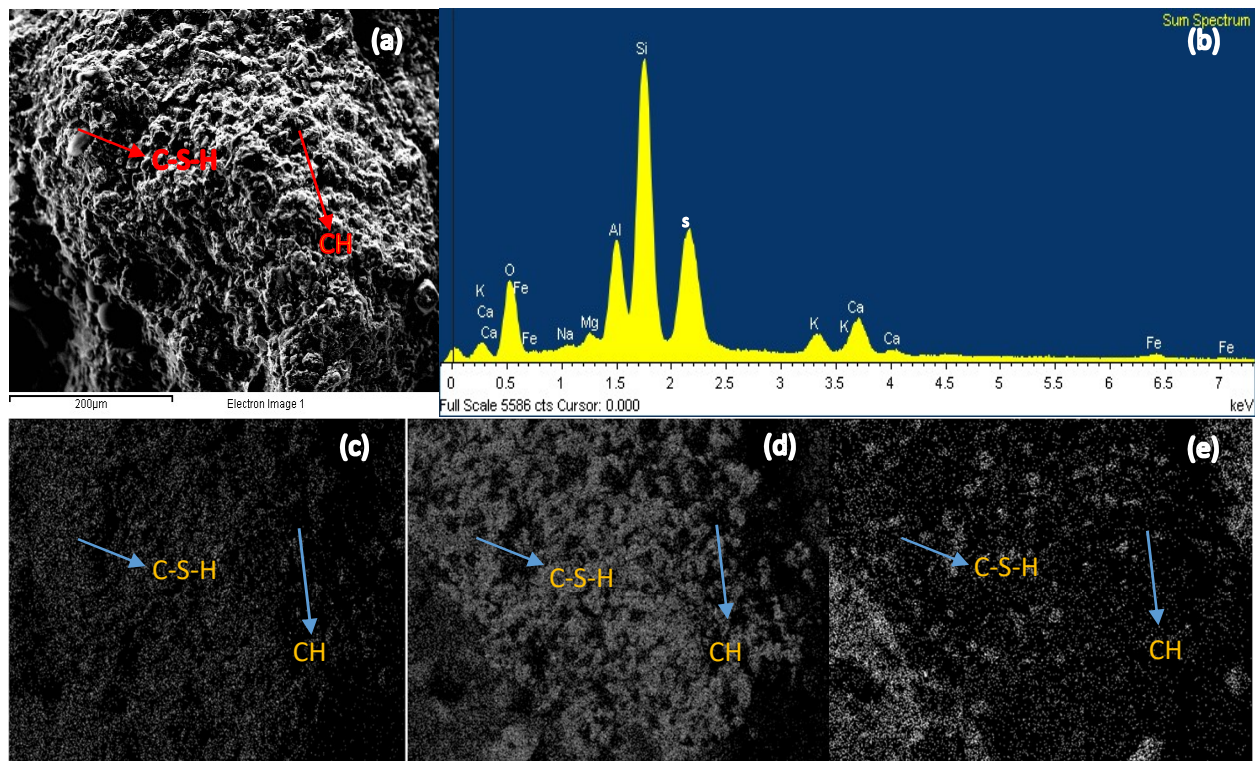


Fig 4.1: EDS analysis of 18-hours sample showing a) Electron image b) EDS spectrum c) Oxygen smart map d) Silicon smart map e) Calcium smart map

4. Discussion

The aim of the EDS investigations was to investigate the spatial distribution of the elements derived from cement Ca, O, Si, Al and Fe. From the smart maps, locations where Si, Ca and O are in abundance represent C-S-H phase. From Fig 4.1b, EDS spectrum shows the presence of Si, Ca and O which can be related to presence

of C-S-H phase in the scan area. Presence of Ca and O attributes to the area with calcium hydroxide(CH). After 18 hours of hydration, 30% of cement particles already reacted to form CH and C-S-H gel. From the evolution, it can be seen that C-S-H grows out from ettringite in form of globules to longer rods. As the hydration time proceeds, the length of rods increases forming “final C-S-H” gel. These evolutions can be seen partly from Fig 3.3. To get a clear idea of the evolution of C-S-H gel, an SEM machine with higher resolutions which can resolve up to a nm should be used. From EDS test conducted on the samples, different types of phases are identified. The C-S-H phase is identified among all the samples and marked so that the PDF measurements can be performed at these locations. This process of identification is discussed more in the next chapter.

CHAPTER V

PAIR DISTRIBUTION FUNCTION ANALYSIS

1. Introduction

SEM/EDS analysis of cement samples couldn't capture the evolution with hydration time on micro scale. Thus, PDF analysis was done to capture the evolution of structure on micro-scale and check if there is any jamming happening during the initial stages of hydration. Due to its heterogeneity and nano-crystalline nature, it is important to characterize this phase along different length scales and structural evolution during the hydration time. In the past, there have been many studies investigating atomic structure and properties of C-S-H using many experimental and theoretical techniques. But, due to C-S-H phase being non-crystalline and heterogeneous, there is a lot of debate still going on. The real structure of a crystal contains significantly more information than the average structure. Careful analysis of subtle details of the real structure proved to explain many properties such as bond order, bond lengths and radial distribution.

In the recent years the pair distribution function analysis of powder samples has become a popular tool for investigating disordered structure. The PDF or radial distribution function(RDF) reveals how the particles (atoms, molecules) are distributed radially from a reference particle. Fig 5.1 shows the principle of PDF. Peaks in PDF are due to the inter-atomic distance, r_i . Scaled by the scattering power of atoms and number of neighboring atoms, peak height, $G(r)$ varies. The PDF reveals the interatomic distances in a material. Diffraction experiments were done at

11-ID-B beamline at Advanced Photon Source(APS), Argonne National Laboratory. Real space analysis for PDF was carried out using fit2D and PDFgetX2 analysis softwares.

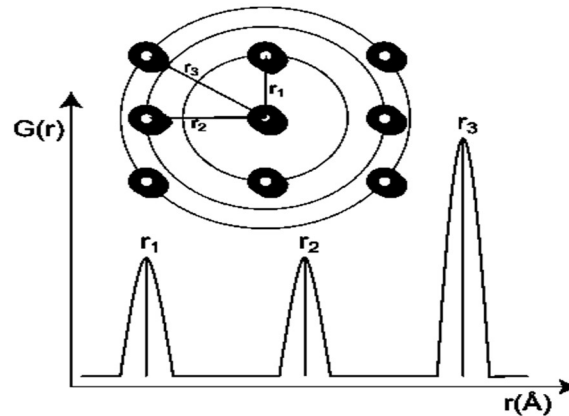


Fig 5.1: Principle of PDF [36]

2. Sample Preparation

The same samples used for SEM and EDS analysis were used for PDF analysis. The mapping of C-S-H phase was done using the SEM at NCF. SEM images and smart maps obtained from EDS for each sample were used for this purpose. 8 samples of different hydration times (18 hours, 1 day, 2 days, 3 days, 4 days, 5 days, 6 days, 7 days) were prepared for PDF analysis.

Mapping of C-S-H:

SEM imaging was done on each sample to identify a representative area. EDS reveals the spectrums and smart maps for scanned area. Fig 5.2 represents the C-S-H mapping procedure for 7-days sample. Fig 5.2(e) represents the phase map from which C-S-H locations were identified for extraction.

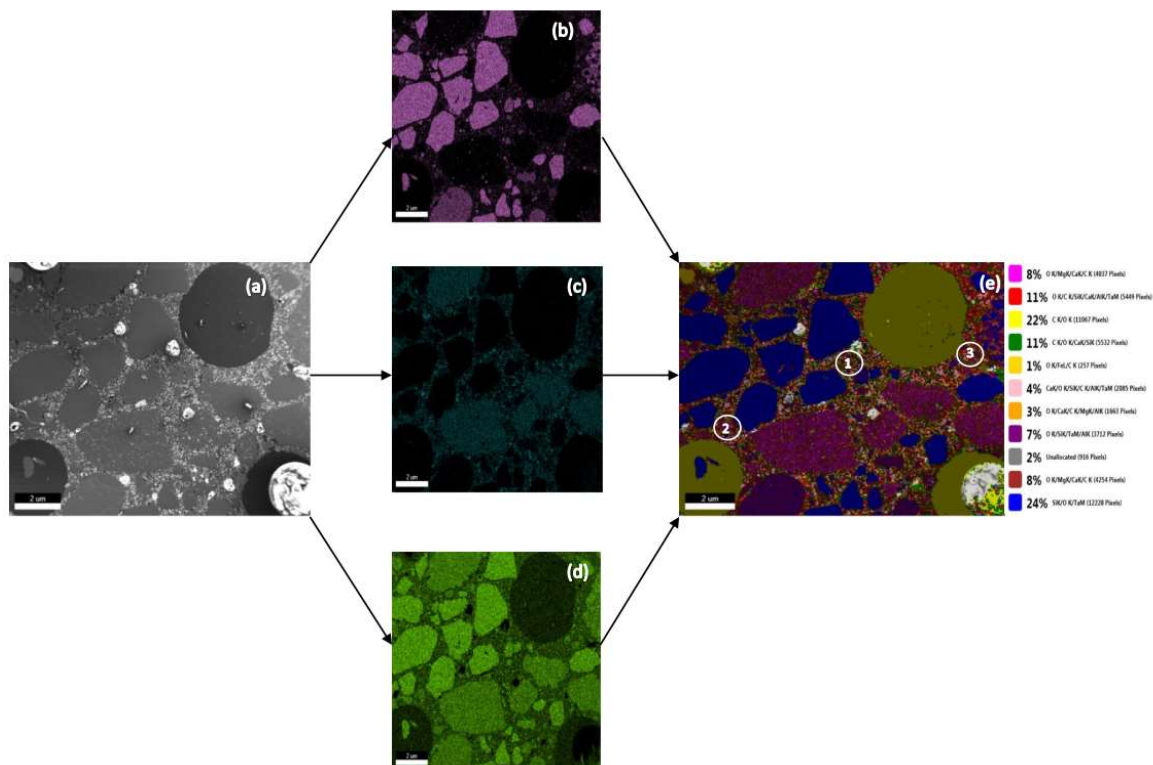


Fig 5.2: C-S-H mapping procedure for extraction representing a) electron image, smart maps of b) Si, c) Ca, d) O, e) total phase map with 1,2,3 representing regions of C-S-H for extraction

EDS spectra obtained were compared with already published spectra [37] C-S-H spectrum to confirm the phase in sample. Once the spectrum was confirmed, relative distance of the area or spot from the center of the sample stage were found out using the JEOL SEM software. Areal analysis gave representative C-S-H spectrum in some samples, thus, there might be other phases present. So, spot analysis was used for all the samples to identify the C-S-H phase. These co-ordinates were noted and marked with a diamond pen precisely to chalk out the identified C-S-H from each sample. An optical microscope at NCF was used to chalk out the marked C-S-H phases and filled into kapton tubings of 0.0435 in. outer diameter. The tubes

were sealed with epoxy on both the ends to prevent entry of moisture and CO₂. Fig 5.3 shows the spot spectrum analysis on a 7-days sample to confirm C-S-H phase.

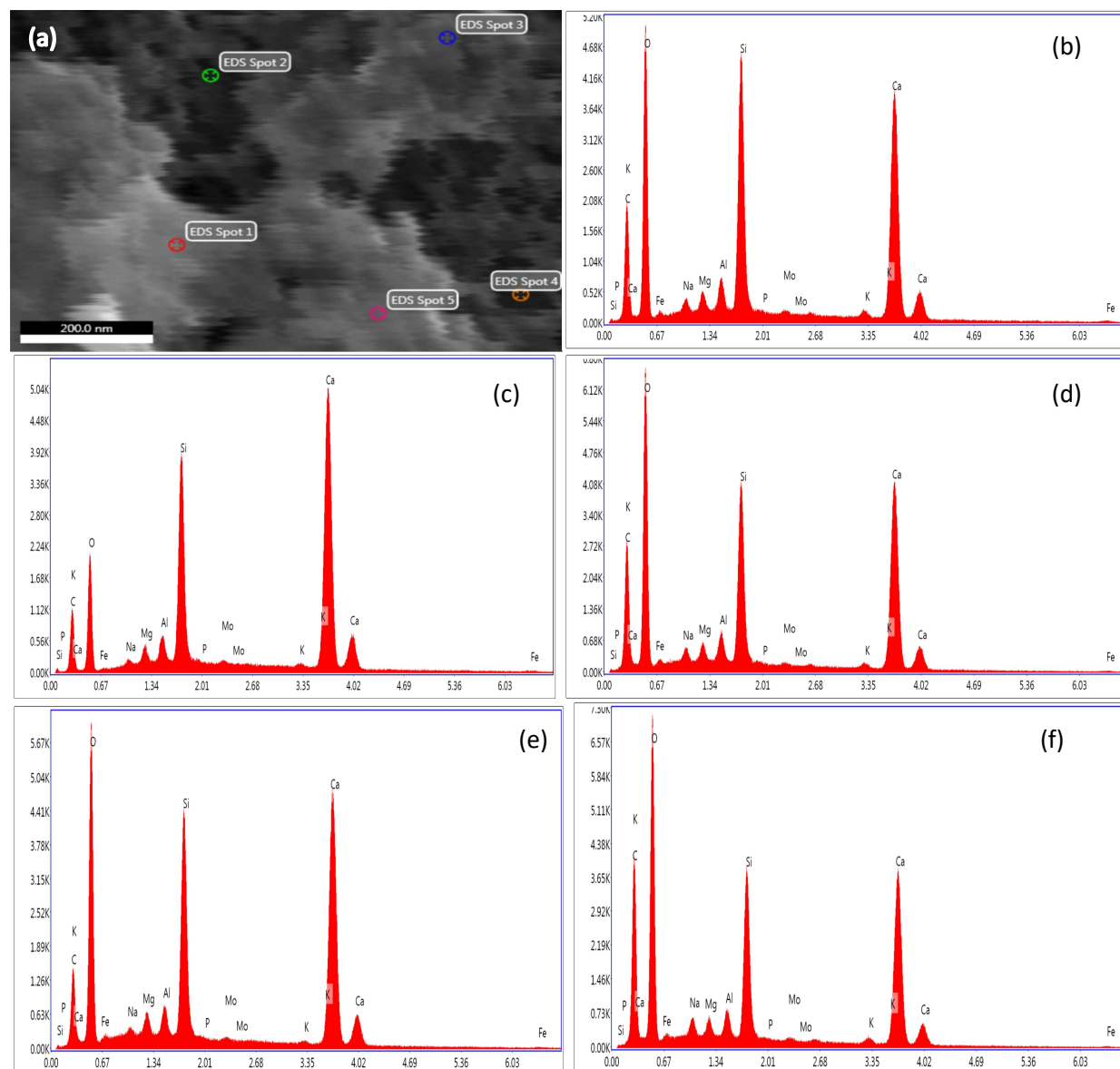


Fig 5.3: EDS spot spectroscopy for identifying C-S-H phases representing a) electron image, b) spot 1, c) spot 2, d) spot 3, e) spot 4, f) spot 5

3. PDF Experimental Procedure

Beamline 11-ID-B is a dedicated PDF beamline operating at fixed energies of 58.66 and 86.7 keV. A refined wavelength of 0.212Å and a two-dimensional Perkin-Elmer amorphous silicon image plate detector 180 mm from sample was used. 8

samples filled in kapton tubings were mounted and aligned according to the hydration times on the sample changer. The sample changer had slots to mount all the samples and run them sequentially as shown in Fig 5.4(b).

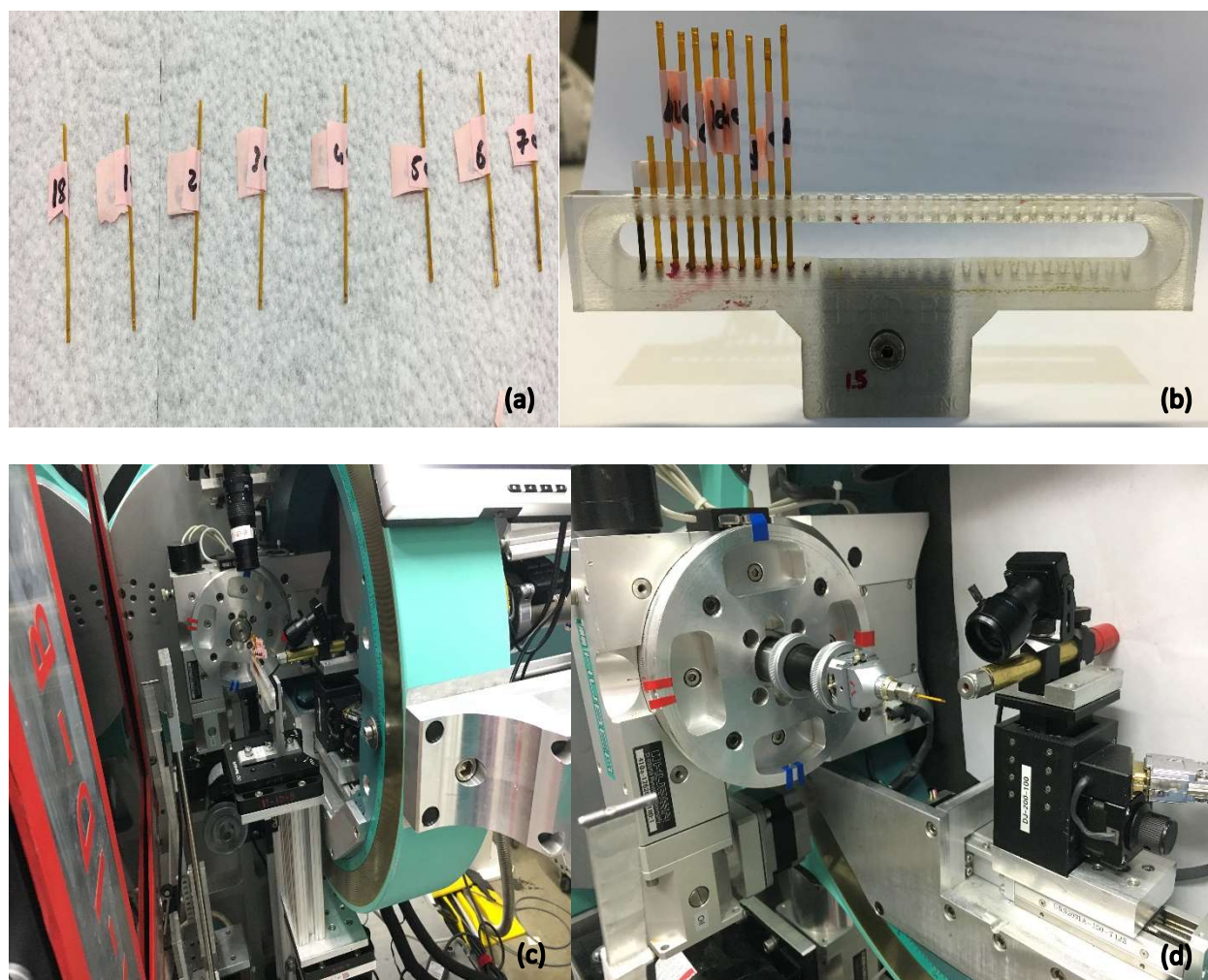


Fig 5.4: a) samples filled in kapton tubes, b) samples mounted in sample changer, c) sample changer mounted on sample stage, d) sample mounted in a rotator

Samples ranging from 18hours-7 days were used for PDF analysis. One sample was analyzed at a time. The sample changer can be moved vertically or horizontally to align each sample with the photon source as shown in Fig 5.4(c). After aligning, the sample was jogged up and down along the photon source to get a better

averaging of the diffraction data. Each sample was analyzed for 2 secs. This process didn't yield visible diffraction data. Then each sample was mounted onto a rotator which can rotate about its horizontal axis as shown in Fig 5.4(d). When the photon source hits the rotating sample, diffraction rings were captured on the detector screen which gets translated onto LINUX workstation running SPEC software. Diffraction data was collected for each sample in the same spinning method. Diffraction data was collected for an empty kapton tube and another with a calibrant Cerium Oxide(Ce_2O_3) to remove the background from the diffraction data. Fit2D was used to convert the data from 2D to 1D.

PDFgetX2 with a Q_{max} of 20 \AA^{-1} was used to obtain the PDF using standard data reduction. Structure factor, $S(Q)$, is a mathematical expression which depicts how a material scatters the incident X-ray, proton or neutron sources. $S(Q)$, is the normalized structure factor obtained from the diffraction experiments (egami and billing 2003). PDF $G(r)$ was directly obtained from the total scattering powder diffraction pattern via a Fourier transform and normalizing total structure factor $S(Q)$ with $Q = 4\pi(\sin \theta)/\lambda$. Equations are indicated below.

$$G(r) = 4\pi r [\rho(r) - \rho_0] \quad (3)$$

$$= \frac{2}{\pi} \int_0^\infty Q [S(Q) - 1] \sin(Qr) dQ \quad (4)$$

Where $\rho(r)$ is the microscopic pair density, ρ_0 is the average number density and Q is the momentum transfer with $Q = 4\pi(\sin \theta)/\lambda$

4. Results:

X-ray PDF plots of samples with different hydration time were obtained. The plots are shown in Fig 5.5. The x axis represents radial distance and y axis represents the PDF. Peaks in the plots are identified based on the PDF measurements of synthetic C-S-H [38]. Structure factor, $S(Q)$ plots are shown in appendix.

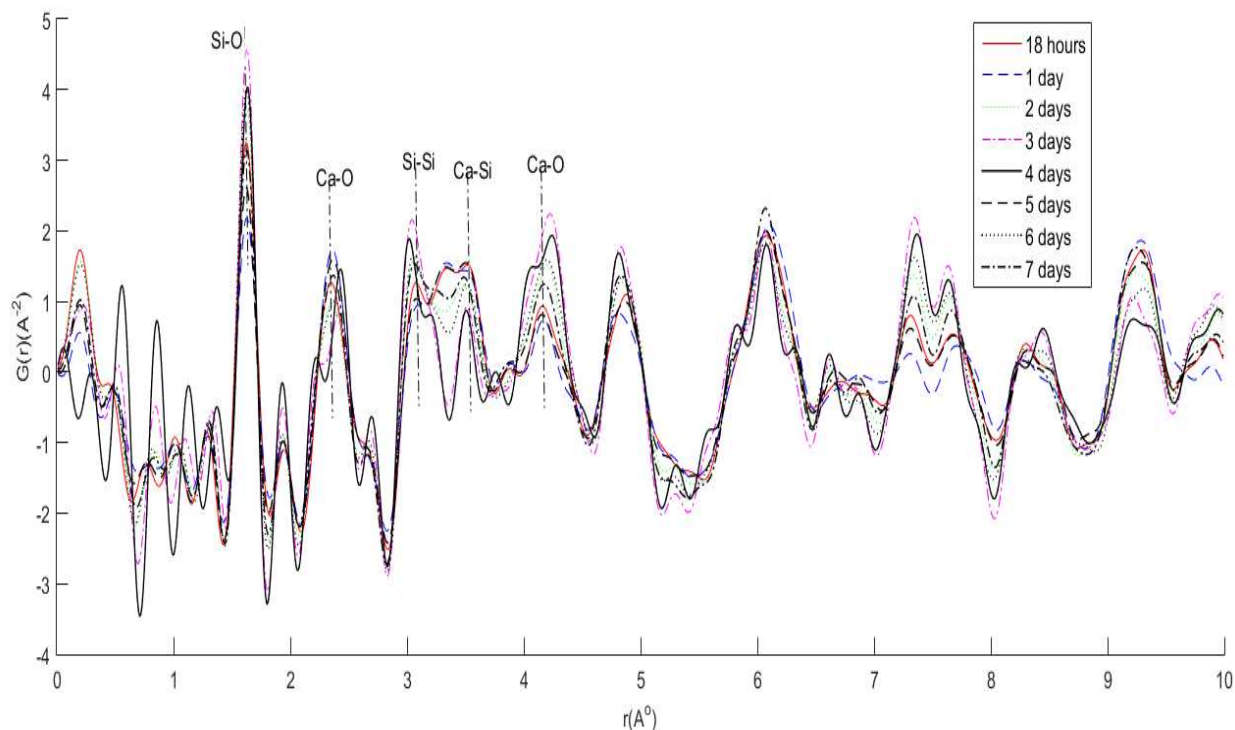


Fig 5.5: Evolution of X-ray Pair Distribution Function (PDF) of C-S-H gel as a function of hydration time with r ranging from 0-10 \AA . Bond peaks are represented by dotted lines.

Peaks are derived from bond lengths of Ca-Si, Ca-O, Si-O. Despite the difference in method of synthesis of C-S-H, bond peaks are obtained at around same order(r). Peaks located at r values below 1.4 \AA are artefacts and due to imperfections and termination errors. Bond lengths of Si-O, Ca-Si, Ca-O are 1.63 \AA , 3.6 \AA , 2.43 \AA respectively. Fig 5.6 shows the peak height evolution of $G(r)$ with hydration time for bonds, Si-O, Ca-Si, Ca-O.

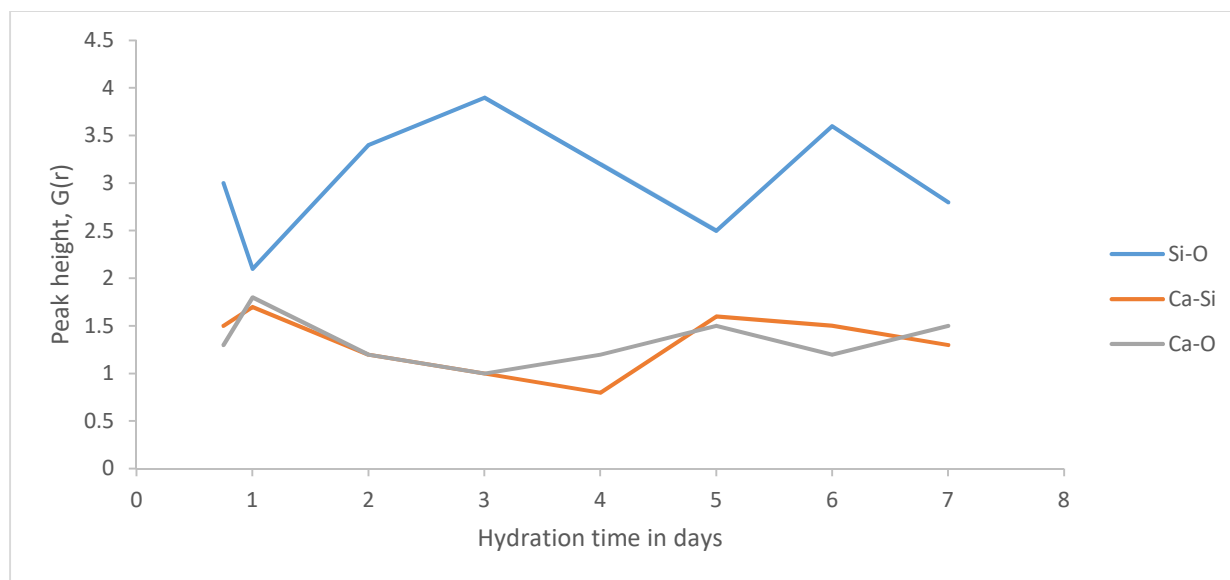


Fig 5.6: Plot showing $G(r)$ peak height evolution with hydration time for Si-O, Ca-Si, Ca-O

5. Discussion

The peaks denoted in Fig 5.5 are in accordance with the PDF measurements from [38]. Si-O peak height varies with hydration time indicating the polymerization of silicate tetrahedron forming silicate chains. Ca-O peaks were observed at two radial distances indicates the presence of calcium octahedral between the layers of silicate chains. This represents the similarities between jennite crystal structure and C-S-H. Fig 5.7 represents the comparison of PDF obtained from this study with PDF of synthetic C-S-H experimentally derived as represented in Monteiro paper [39]. From Fig 5.7, it can be seen that the Si-O bond peaks are formed at 0.16nm for both the Monteiro data and data from APS. The same is observed for Ca-O at 0.3nm but $G(r)$ is greater for the Monteiro data. The rest of the bond peaks for Si-Si and Ca-Si are formed at slightly different radial distance with same $G(r)$. Figure 5.8 represents the short-range order in C-S-H gel. From Fig 5.6, a trend is observed between peak

heights of Si-O and Ca-O, they are inversely proportional to each other. During 18 hours-1 day, decrease in Si-O peak height and increase in Ca-O peak height indicates the formation of layered structure. This means that 18-24 hours period is dynamic state with formation of micro-structure.

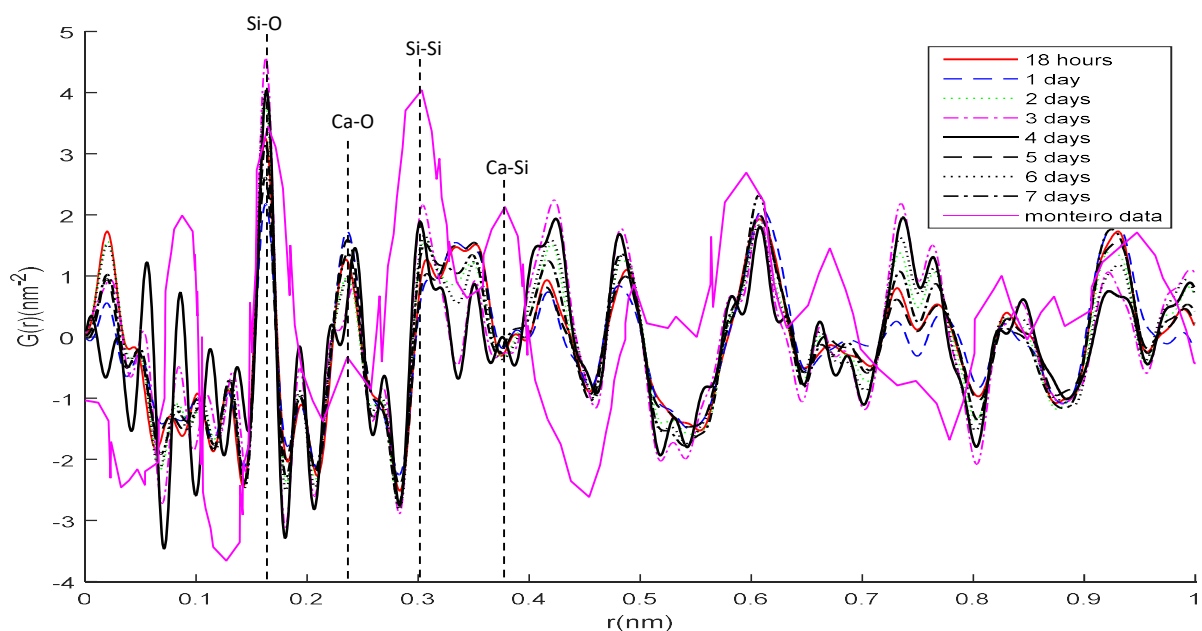


Fig 5.7: Comparison with Monteiro experimental data

Overall, the data from both appear to be the same with almost the same number of bond peaks and slightly different radial distance. Lack of well-defined (sharp) peaks denote that the structure is not truly amorphous or fully crystalline. C-S-H phase in cement is neither amorphous nor crystalline. This makes the structural identification difficult for C-S-H phases. The presence of other crystalline phases in the sample will contribute to local structuring order/dis-order. The crystalline contributions will also influence the longer range ordering, and therefore explains the increase in some of the atom-atom intensities from Monteiro data. At the very initial stages of hydration, measurements of X-ray PDF of C-S-H

gel reveals that the data is dominated by water containing atom-atom correlations due to large amount of water adsorbed in the sample. When the atomic ordering of C-S-H gel as the hydration proceeds is compared with the final C-S-H gel atomic ordering from literature, it is revealed that the hydration process did not adversely affect the atomic structure of the gel. Jamming trend could not be quantified from PDF results.

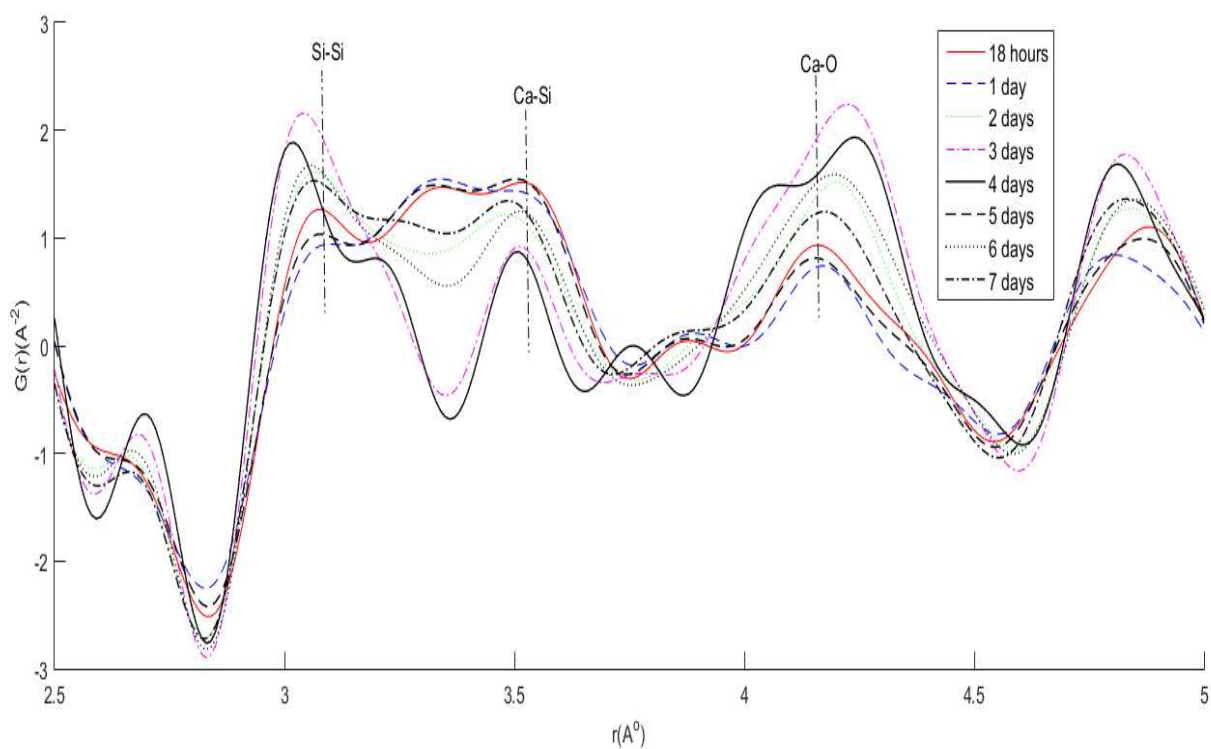


Figure 5.8: PDF of C-S-H gel with r ranging from 2.5-5 \AA^0 to clearly observe the evolution of peak heights as a function of hydration time.

CHAPTER VI

Nuclear Magnetic Resonance Spectroscopy

1. Introduction

Results from PDF couldn't give detailed information about the crystal structural arrangement in cement samples. Previous studies on cement using ^{29}Si NMR on cement hydrates proved to be an efficient way to evaluate the basic structure of C-S-H on atomic scale. Also confinement was introduced in the samples to see if there would be any effect of confinement during early stages of hydration.

Principle of NMR is, when the nuclei of atoms are immersed in a magnetic field, absorb and reemit electromagnetic radiation. Based on the strength of magnetic field and magnetic properties of isotopes of atoms, they resonate at a certain frequency. Based on the spin properties of the nuclei, some experience this phenomenon and others do not. Matter is composed of molecules, molecules are composed of atoms, each atom has an electron cloud around it and in the center are protons along with neutrons. In C-S-H all the atoms have nuclear isotopes detectable by NMR: ^{29}Si , ^1H , ^{43}Ca , ^{17}O [40].

NMR spectroscopy is the application of this NMR technique to study various properties of matter: physical, chemical and biological. This makes NMR spectroscopy one of the widely used application in scientific studies. Time domain NMR spectroscopic techniques are used to study molecular dynamics in solutions. Solid state NMR spectroscopy is used to investigate the molecular structure of solids.

Solid state NMR employs different nuclei (^1H , ^{17}O , ^{27}Al , ^{29}Si) probes. ^{29}Si NMR method was employed for this study. NMR experiments were done at Intertek Laboratories, Allentown, PA. Confinement was introduced during sample preparation to investigate how C-S-H grows in confined space, similar to what occurs during hydration in pore spaces.

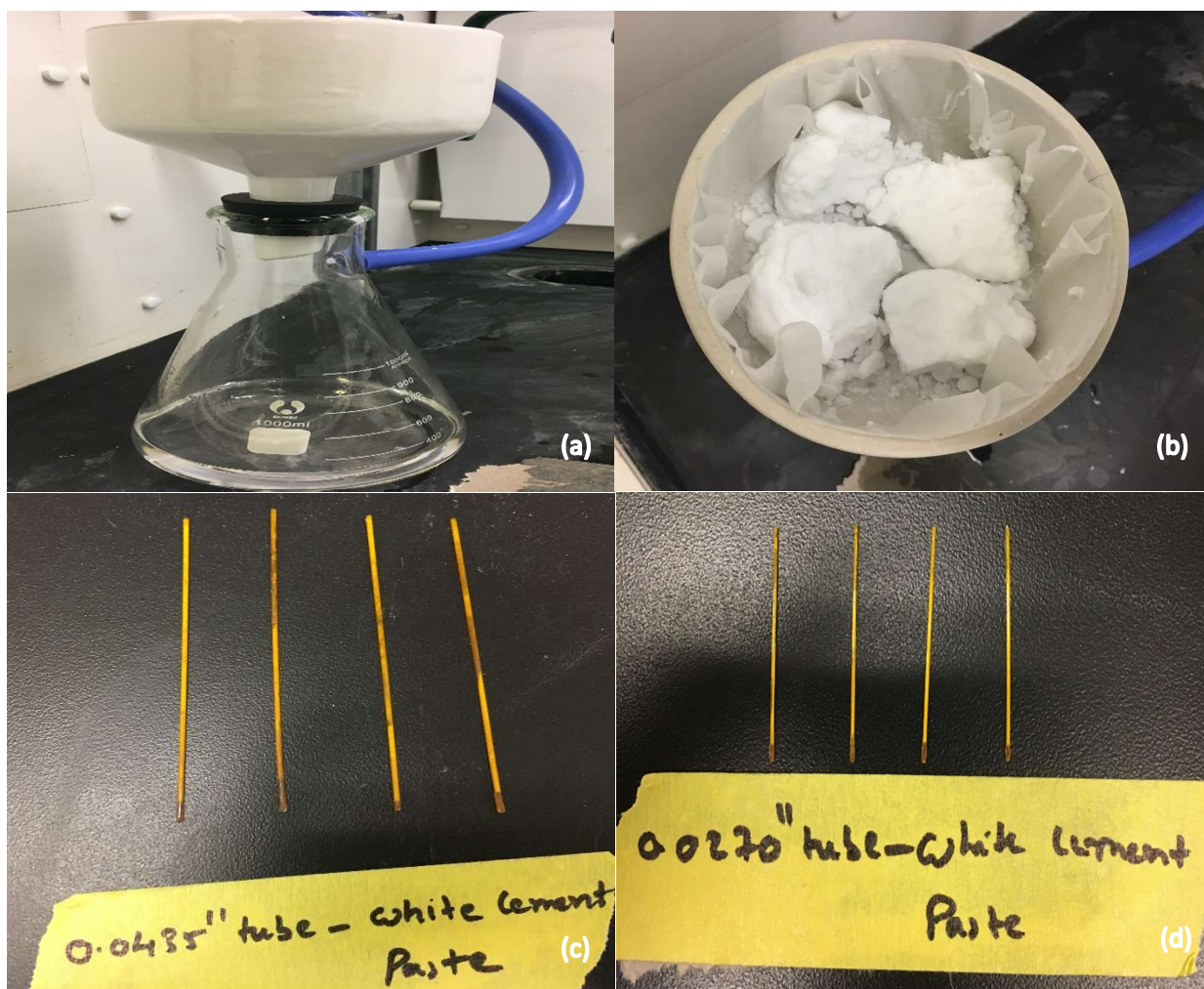
2. Sample Preparation

Two types of samples were used for the study, lab made synthetic C-S-H and white cement paste (WCP) to limit the iron(Fe) during the NMR experiment. The iron(Fe) present in ordinary Portland cement paste can affect the magnet in the NMR machine. The sample were confined in two different sizes of Kapton tubes: 0.0435" and 0.0270". A water to cement ratio of 0.5 was used for making white cement samples. Cement and water were introduced into the tubes using a micro pipette(0.5-10ul) and syringes (1 ml gastight with luer tip). The sample was hydrated in the tubes for 3 days before hydration stop was done. The tubes were cut and white cement paste was removed from the tubes. Hydration was stopped using the solvent exchange method as explained in SEM section.

3. Synthesis of C-S-H

0.1-mole of reagent grade granular Sodium Silicate($\text{Na}_2\text{SiO}_3 \cdot 5\text{H}_2\text{O}$) was dissolved in 242 mL of carbon dioxide-free deionized water. Then 0.1 moles of reagent grade Calcium Nitrate($\text{Ca}(\text{NO}_3)_2 \cdot 4\text{H}_2\text{O}$) that was dissolved in 250 mL of carbon dioxide-free deionized water and added to the sodium silicate solution. After both the solutions were added together, stirring was done for 1.5 hours in a parafilm sealed

plastic container to facilitate good mixing [41]. A white precipitate starts to form during mixing, which is C-S-H gel. 0.17g lime (CaO) was dissolved in 2L deionized water to make the rinse solution. A Buchner funnel system connected to vacuum was used to wash C-S-H with rinse solution as shown in Fig 6.1(a) to remove excess water in the gel. After the rinse solution was completely added to the C-S-H solids, the sample was tightly sealed in a plastic container with parafilm to avoid entry of CO₂ and moisture. The C-S-H precipitate had a Ca/Si ratio of 1. Synthetic C-S-H was filled in two different sizes of Kapton tubes shown in Fig 6.1(c)-6.1(f)



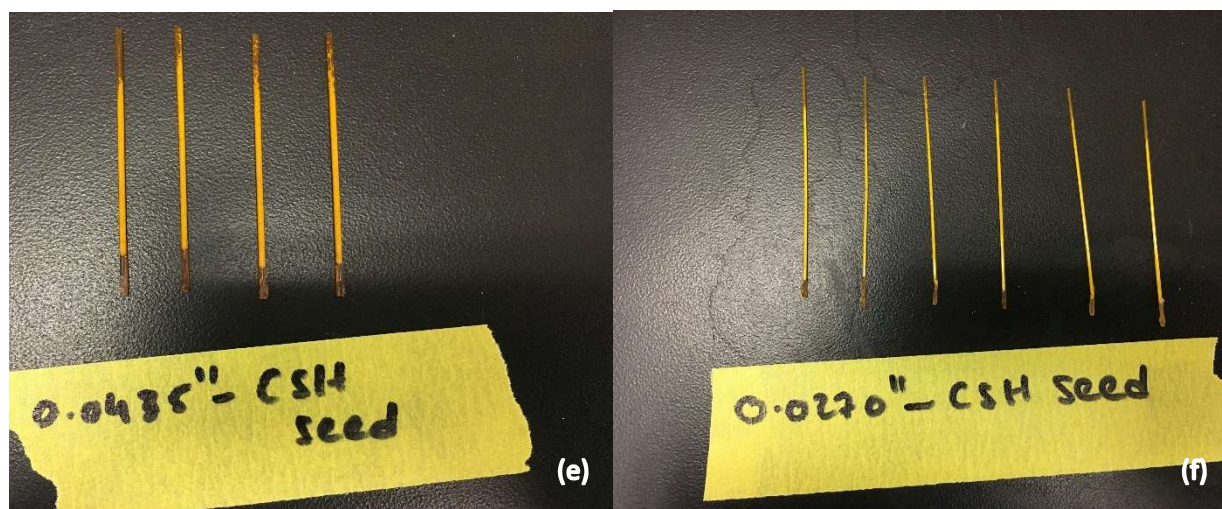


Fig 6.1: a) Buchner funnel system for filtration, b) C-S-H seed after filtration, WCP in kapton tubes of c) 0.0435" d) 0.0270", C-S-H seed in kapton tubes of e) 0.0435", f)0.0270"

Inductively coupled plasma atomic emission spectroscopy (ICP-AES) was done on both white cement and synthetic C-S-H to find the trace elements and characterize the sample before the NMR spectroscopy. Drift, digest and dilution correction factors were applied to the results. The Detection Limit (DL) of the machine was 0.045 ppm for Mg. Table 2 shows the ICP-OES results for both the samples. There was very little Fe and less than 0.045 ppm of Mg present in synthetic C-S-H seed.

Sample- tube size	Si ppm	Fe ppm	Mg ppm	Ca ppm	Al ppm	K ppm
WCP- 0.0435"	82285	1417	3351	340967	18358	2318
WCP- 0.0270"	84685	1386	2719	329614	18223	1666
C-S-H seed- 0.0435"	82149	59	DL	80738	153	914
C-S-H Seed- .0270"	84612	75	DL	82960	115	699

Table 2: ICP-OES characterization

4. ²⁹Si NMR Experimental Procedure

²⁹Si NMR was done at Intertek Laboratories, Allentown, PA. The samples were packed into a 7 mm diameter zirconium oxide rotor. The packed rotor was then sealed

with a Kel-F cap. Solid state ^{29}Si NMR spectra were obtained at ambient temperature on a Bruker Avance II 300 FT-NMR spectrometer, equipped with a 7 mm MAS probe. The acquisition was carried out using one pulse employing a 10 second recycle delay while the rotor was spun at 5000 Hz at magic angle. Detailed NMR report is shown in appendix

5. Results

Fig 6.2 and Fig 6.3 show the spectra for white cement paste and synthetic C-S-H respectively for different confinements. All the peaks are in the regions typically associated with Silicon bound to four Oxygen. The analysis is based on the Q^n classification [42] where Q represents SiO_4^{4-} (silicate tetrahedron) unit, n represents degree of connectivity of oxygen between the SiO_4^{4-} - units.

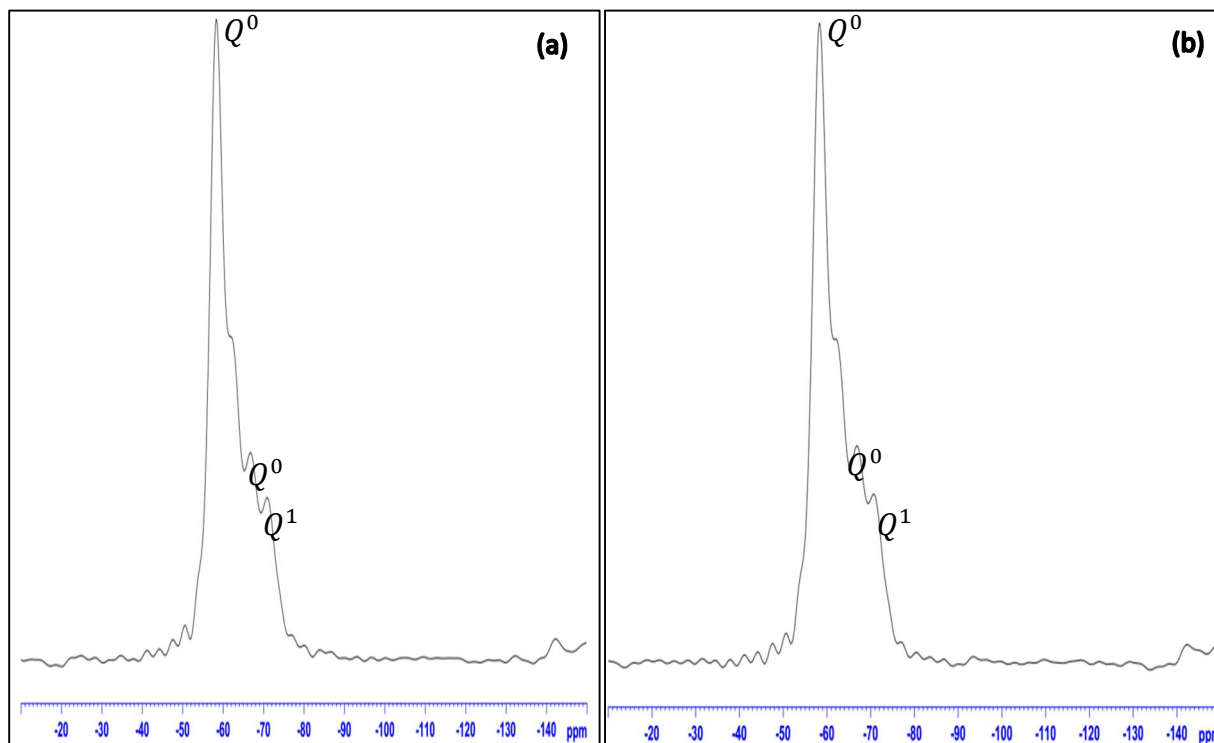


Fig 6.2: NMR spectra for WCP confined in kapton tube of size a) 0.0435", b)0.0270"

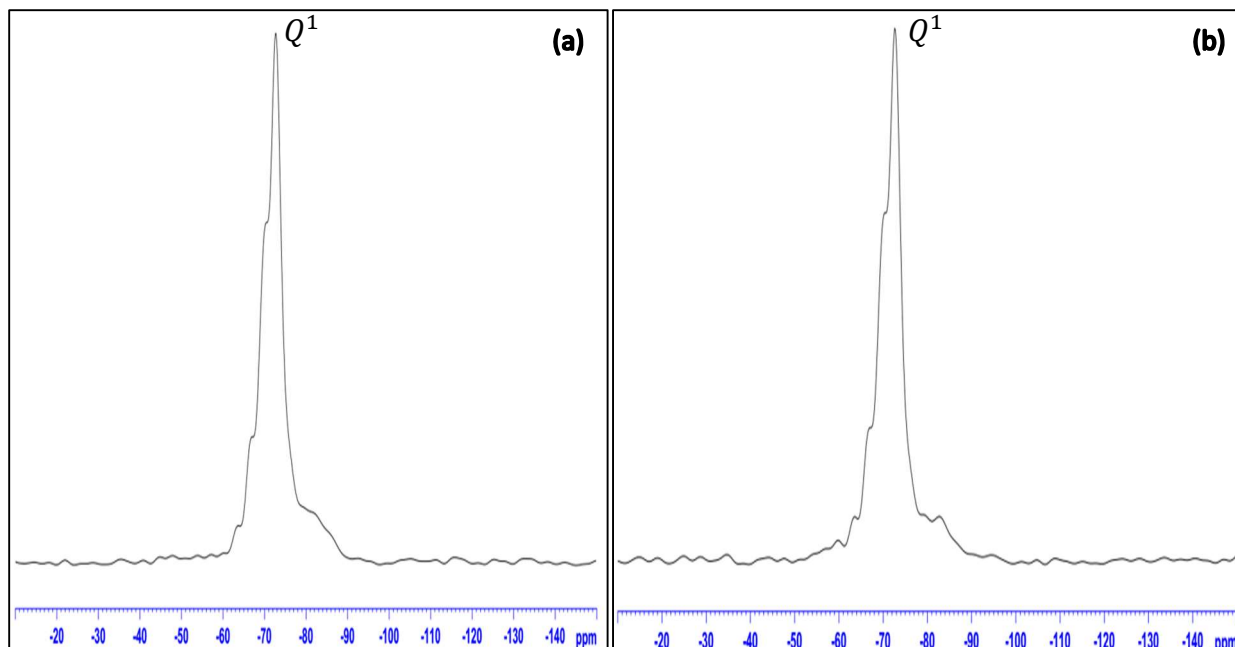


Fig 6.3: NMR spectra for synthetic C-S-H confined in kapton tube of size a) 0.0435", b) 0.0270"

6. Discussion

Q^0 represents that there is no polymerization happening during the hydration time and SiO_4^{4-} starts to form. It also represents the presence of anhydrous C_3S during the hydration. Peak Q^1 attributes to end-chains tetrahedra where SiO_4^{4-} is chained to one SiO_4^{4-} . Peak Q^2 attributes to middle chain tetrahedra where SiO_4^{4-} is chained to two more SiO_4^{4-} . Q^2 also represents the bridging tetrahedras between two layers of C-S-H.

From fig 6.2, for WCP samples, two sharp Bragg's peaks are observed for Q^0 at 58 and 67ppm, Q^1 peak is observed at 71ppm. As the samples were hydrated for 3 days, Q^0 represents anhydrous C_3S and Q^1 represents polymerization of silicate chains. From fig 6.3, for C-S-H samples, one sharp Q^1 peak is at 73ppm which shows that there are only end chain silicon terahedras and polymerization happens between

them. Absence of Q^2 peaks in both WCP and synthetic C-S-H may be due to high Ca/Si ratio. With decrease in Ca/Si ratio, Q^2 peak starts to appear[43]. It has been shown that Ca/Si ratio is dependent on concentration of calcium and silicate ions in the reagent solutions even before C-S-H precipitation, making the initial concentrations as key parameters for controlling C-S-H structure. Secondary parameters such as temperature, carbonation, addition of silica fume can change the concentration of ions thereby influencing Ca/Si ratio and length of the chains in final C-S-H gel. For Ca/Si ratio smaller than 0.66, silicate chains can get linked which leads to more polymerization and increasing the strength of the C-S-H structure.

The solid state ^{29}Si NMR spectra of both white cement samples are identical, indicating that the ^{29}Si environment of both the samples are the same. Similarly, the solid state ^{29}Si NMR spectra of both the synthetic C-S-H samples show that C-S-H samples also have very similar ^{29}Si structures. The ^{29}Si NMR resonance signals of the C-S-H samples are located at the higher field side of the spectrum compared to that of the white cement paste samples, which suggests significant differences in the ^{29}Si environment between these two groups.

CHAPTER VII

Conclusions and Future work

1. Overview

Key conclusions from this study are:

- The jamming trend proposed in molecular dynamics could not be experimentally confirmed using the experimental methods.
- SEM/EDS can be used in conjunction with PDF analysis to study unique phases of heterogeneous materials.
- ^{29}Si NMR results shows that synthetic C-S-H and white cement paste have similar Si environments with a difference in polymerization of silicate chains
- Confinement of white cement and C-S-H samples down to 0.0270" has no effect on hydration process.

In this work, experimental methods are done for cement and cement-based materials to understand the intrinsic building block of cement at different length scales. An attempt to grow the cement in a confined space to introduce jamming during the hydration process is also done. Experiments across different length scales and how to interpret results from one experiment to lay a foundation for next experiment is also done. Combination of synchrotron-based PDF and ^{29}Si NMR with electron microscopic studies (BSE, EDS) helps to carry out micro-scale studies on cement matrix. All the techniques (SEM, EDS, PDF, ^{29}Si NMR) adopted in this study has unique capabilities and, used in a complementary way, allows to investigate the phases, elemental distribution, and structural properties to be determined on the same investigated area. This helps in understanding the structure of C-S-H on macro,

micro and nano scale and co-relate the evolution on each length scale. More conclusions from each study and future scope of the work are presented below.

2. Conclusions from SEM/EDS

The application of SEM enhances our ability to understand the microstructure of C-S-H. SEM technique helps in imaging the intricate microstructure of cement samples on a micro scale. Samples should be prepared carefully as backscattered electron and x-ray imaging requires highly polished surface. Combining backscattered electron and X-ray images, different phases present in cement and cement materials can be identified accurately.

In this study, SEM was used to investigate the growth of cement on 1um, 10um and 100um. Evolution of C-S-H phase from globular to fibrillary with hydration time was observed on 10um length scale. Images from SEM helps in narrowing down the EDS locations for obtaining element maps and distribution. With more technical developments in SEM capabilities, spatial resolution of the images can be reduced from micro-scale to nano-scale. This technological advancement will enable to investigate the nano-particle systems in cement and cementitious materials.

In this study, EDS was used to obtain spectra to identify the chemical composition of sample area. Different types of analysis (spot, line and areal spectrum) helps in obtaining representative spectra for the sample. Elemental maps help in identifying C-S-H and $\text{Ca}(\text{OH})_2$ evolution with time. EDS proved to be an efficient way to identify particular phases in a sample. It also helps in characterizing the elemental composition of a sample.

3. Conclusions from PDF

PDF analysis was done on samples containing C-S-H phases identified by EDS on cement samples hydrated for particular time. This was done to replicate the natural environment of C-S-H rather than lab made synthetic C-S-H. It was observed that C-S-H evolves in sheet like structure close to jennite crystal, but C-S-H structure is neither crystalline nor amorphous. The presence of other crystalline phases in the sample contributes to local structuring order/dis-order. From the PDF evolution with hydration time, the atomic order of C-S-H didn't change adversely from the initial order. This may be due to high Ca/Si ratio in samples. Calcium and silicon influence the cluster morphologies in different ways: the former contributes to an ordered structure while the latter increases the amorphous state of the structure. Furthermore, a wide range of calcium/silicon ratios should be taken into consideration to observe morphology evolution. In this study, PDF couldn't clearly explain the order/disorder in C-S-H structure. Therefore, in-situ imaging techniques in conjunction with PDF would be able to capture the intricate structure of C-S-H on atomic scale.

4. Conclusions from ^{29}Si NMR:

Effect of confinement was investigated on white cement and lab made synthetic C-S-H by ^{29}Si NMR technique. For white cement, peaks were observed for Q^0 and Q^1 indicating the presence of anhydrous C_3S and polymerization of silicate chains respectively. Q^1 peak in synthetic C-S-H sample indicates the presence of only silicate tetrahedron and polymerization between them. Synthetic C-S-H have similar

Si environment to white cement. All of the peaks are in a region typically associated with silicon bound to four oxygen atoms. The difference between the two sets of samples may be in the extent of hydration or the number of hydroxyls (versus $-\text{OSi}$) bound to silicons. There was no effect of confinement on both the samples, indicating that the samples should be confined on a scale equivalent to C-S-H structure ($\sim 5\text{nm}$) to show the effect of confinement. However, these NMR results helped in confirming that the white cement paste and synthetic C-S-H have very similar Si environment and they can be compared for future studies.

5. Future Work

All the above experiments did not give a clear picture of structure evolution with hydration. In-situ image observations along with the above results would help understand the structure of C-S-H better. Numerical models have been used to simulate the evolution of the C-S-H structure with limited consideration of geometry (spheres). Conclusions from these numerical models would be confirmed by observing the evolution using transmission electron microscope (TEM). Effect of jamming/confinement on the micro structure evolution of C-S-H particles ($\sim 5\text{nm}$) will be investigated by introducing the C-S-H particles in a liquid cell and in-situ hydration of particles. This process is called liquid cell microscopy. C-S-H and white cement samples for TEM observation will be prepared using TEM sample preparation. White cement samples would be varied from 1day-7days of hydration time. In-situ liquid cell TEM observation of synthetic C-S-H sample would be done for continuous 0-20 hours hydration time. Confinement would be achieved by

introducing the C-S-H particles in liquid cell at a controlled membrane distances of 50nm, 100nm. From this experiment, we expect to obtain a clear structural evolution of C-S-H with hydration time and also the effect of confinement, compare with PDF and NMR studies already done. Our proposal for TEM and liquid cell microscopy testing at Center for Integrated Nanotechnologies(CINT), Sandia National Laboratories got accepted. Fig 7.1 represents the testing procedure.

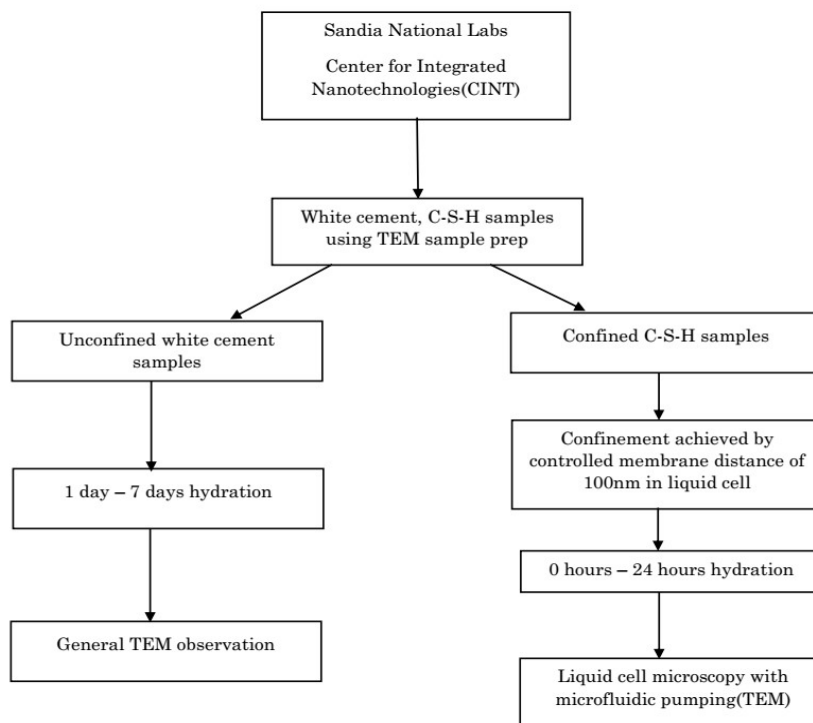


Fig 7.1 : Testing procedure for TEM/liquid cell microscopy

BIBLIOGRAPHY

- [1] National Ready Mixed Concrete Association, "Concrete CO₂ Fact Sheet," NRMCA, 2008.
- [2] Bielo, D., "Cement from CO₂: A Concrete Cure for Global Warming?," *Scientific American*, 2008.
- [3] Al-Tabbaa, A., "The concrete that heals its own cracks," *World Economic Forum*, 2016.
- [4] Jennings, H. M., Tennis, P. D., "Model for the developing microstructure in Portland cement pastes," *J Am Ceram Soc*, vol. 77, no. 12, pp. 3161-3172, 1994.
- [5] Thomas, J.J., Jennings, H.M., "The surface area of cement paste as measured by neutron scattering: evidence for two C-S-H morphologies," *Cem Concr Res*, vol. 28, no. 6, pp. 897-905, 1998.
- [6] Fonseca, P.C., Jennings, H.M., Andrade J.E., "A nanoscale numerical model of calcium silicate hydrate," *Mechanics of Materials*, vol. 43, no. 8, pp. 408-419, 2011.
- [7] Brunauer, S., "Tobermorite Gel- The Heart of Concrete," *Research and Development Laboratories of the Portland Cement Association*, vol. 50, no. 1, pp. 210-229, 1962.
- [8] Zhang, L., "The structure study of calcium silicate hydrate (C-S-H) (QE report)," Hong Kong University of Science and Technology, Hong Kong, 2012.
- [9] Taylor H., *Cement Chemistry*, vol. 2, London: Academic Press, 1997.
- [10] Bishop, M., Bott, S. G., Barron, A. R., "A new mechanism for cement hydration inhibition: solid-state chemistry of calcium nitrilotris(methylene) triphosphonate," *Chemistry of Materials*, vol. 15, no. 16, pp. 3074-3088, 2003.
- [11] Richardson I., "The nature of calcium silicate hydrate," *Cement and Concrete*, vol. 29, pp. 1131-1147, 1999.
- [12] Groves, G., "TEM studies of cement hydration," in *Mater. Res. Soc. Symp. Proc.85*, 1987.
- [13] Gmira, A., "Etude textural et thermodynamique d'hydrates modeles du ciment," Universite D Oriens. PhD Thesis, France, 2003.
- [14] Hamid, S., "The crystal structure of the 11 A natural tobermorite Ca_{2.25}Si₃," *Zeitschrift für Kristallographie*, vol. 154, no. 3-4, pp. 189-198, 1981.
- [15] Bonaccorsi E., Merlino, S., Taylor, H., "The crystal structure of Jennite Ca₉Si₆O₁₈(OH)₆ 8H₂O," *Cement and Concrete Research*, vol. 34, no. 9, pp. 1481-1488, 2004.
- [16] Merlino, S., Bonnacorsi, E., Armbruster, T., "The real structure of tobermorite," *European Journal of Mineralogy*, vol. 13, no. 3, pp. 577-590, 2001.

- [17] Shahsavari, R., Buechler, M. J., Pellenq, R. J. M., Ulm, F. J., "First-principles study of elastic constants and interlayer interactions of complex hydrated oxides: case study of tobermorite and jennite," *Journal of American Ceramic Society*, vol. 92, no. 10, pp. 2323-2330, 2009.
- [18] Nomat, A., "The structure and stoichiometry of C-S-H," *Cement and Concrete*, vol. 34, pp. 1521-1528, 2004.
- [19] Costantinide, G., Ulm, F., "The nanogranular nature of C-S-H," *Journal of*, vol. 55, no. 1, pp. 64-90, 2006.
- [20] Allen, A. J., Thomas, J. J., Jennings, H. M., "Composition and density of nanoscale calcium silicate hydrate in cement," *Nature material*, vol. 6, pp. 311-316, 2007.
- [21] Garbev, K., Bornefeld, M., Beuchle, G., Stemmermann, P., "Cell Dimensions and Composition of Nanocrystalline Calcium Silicate Hydrate Solid Solutions. Part 2: X-Ray and Thermogravimetry Study," *Journal of the American Ceramic Society*, vol. 91, no. 9, pp. 3015-3023, 2008.
- [22] Renaudin, G., et al., "Structural characterization of C-S-H and C-A-S-H samples Part II: Local environment investigated by spectroscopic analysis," *Journal of Solid State Chemistry*, vol. 182, no. 12, pp. 3320-3329, 2009.
- [23] Brunauer, S., Kantro, D. L., Copeland, L. E., "The stoichiometry of the hydration of β -dicalcium silicate and tricalcium silicate at room temperature," *Journal of the American Chemical Society*, vol. 80, no. 4, pp. 761-767, 1958.
- [24] Jennings H. M., "Refinements to colloid model of C-S-H in cement: CM II," *Cement and Concrete Research*, vol. 38, no. 3, pp. 275-289, 2008.
- [25] Powers, T., Brownyard, L., "Studies of the physical properties of hardened Portland cement paste," *ACI Journal Proceedings*, vol. 43, 1946-1947.
- [26] Jennings, H.M., "A model for the microstructure of calcium silicate hydrate in cement paste," *Cement and Concrete Research*, vol. 30, pp. 101-116, 2000.
- [27] Chen, J., Thomas, J., Taylor, H. & Jennings, H.M., "Solubility and structure of calcium silicate hydrate," *Cement and Concrete Research*, vol. 34, no. 9, pp. 1499-1519, 2004.
- [28] Grangeon, S., et. Al., "On the nature of structural disorder in calcium silicate hydrates with a calcium/silicon ratio similar to tobermorite," *Cement and Concrete Research*, vol. 52, pp. 31-37, 2013.
- [29] Taylor, H. F. W., Howison, J. W., "Relationships between calcium silicates and clay minerals," *Clay Miner. Bull*, vol. 3, pp. 98-111, 1956.
- [30] Taylor, H. F., "Proposed structure for calcium silicate hydrate gel," *Journal of the American Ceramic Society*, vol. 69, no. 6, pp. 464-467, 1956.
- [31] Pellenq R.J., "A realistic molecular model of cement hydrates," *Proceedings of the National Academy of Sciences*, vol. 106, no. 38, pp. 16102-16107, 2009.
- [32] JEOL SEM, "JEOL USA Electron Optics Documents," 25 06 2009. [Online]. Available: <http://www.jeolusa.com/DesktopModules/Bring2mind/DMX/Download.aspx?>

- EntryId=598&Command=Core_Download&language=en-US&PortalId=2&TabId=320.
- [33] Knapen, E., Cizer, O., Van Balen, K., Van Gemert, D., "Comparison of Solvent Exchange and Vacuum Drying Techniques to Remove Free Water From Early Age Cement-Based Materials," in *2nd International Symposium on Advances in Concrete through Science and Engineering* , Quebec City, Canada, 11-13 September, 2006.
 - [34] Paul, E. Stutzman, James, R. Clifton, "Specimen Preparation for Scanning Electron Microscopy," *Proceedings from Twenty-First International Conference on Cement Microscopy*, pp. 10-22, 1999.
 - [35] Essential Knowledge Briefings, Energy Dispersive Spectroscopy, West Sussex: John Wiley & Sons Ltd., 2015.
 - [36] Karsten, K., Bernd H., Bruker AXS, "Determination of Pair Distribution Functions(PDF)," Bruker AXS, Madison, WI, USA, 2009.
 - [37] Winter, N. B., Scanning Electron Microscopy of Cement and Concrete, Suffolk, UK: WHD Microanalysis Consultants Ltd., 2012.
 - [38] Antoine, E. Morandea, Claire, E. White, "In situ X-ray pair distribution function analysis of accelerated carbonation of a synthetic calcium-silicate-hydrate gel," *Journal of Materials Chemistry*, vol. 3, pp. 8597-8605, 2015.
 - [39] Skinner, L. B., Chae, S. R., Benmore, C. J., Wenk, H. R., Monteiro, P. J. M., "Nanostructure of Calcium Silicate Hydrates in Cements," *Physics Review Letters*, vol. 104, no. 19, p. 195502(4), 2010.
 - [40] Colombet, P., Grimmer, A.R., Zanni, H., Sozzani, P., "Nuclear Magnetic Resonance Spectroscopy of Cement-Based Materials," in *Springer*, Bergamo, 1996.
 - [41] Chen, Jeffrey J., Thomas Jeffrey J., Taylor, Hal F. W., Jannings Hamlin M., "Solubility and Structure of Calcium Silicate Hydrate," *Cement and Concrete Research*, vol. 34, no. 9, pp. 1499-1519, 2004.
 - [42] Engelhard, G., Michel, D., 29Si NMR of Silicates and Zeolites, Chichester: John Wiley, 1987.
 - [43] Zanni, H., Rassem-Bertolo, R., Masse, S., Fernandez, L., Mieto, P., Bresson, B., "A Spectroscopic NMR Investigation of the Calcium Silicate Hydrates Present in Cement and Concrete," *Magnetic Resonance Imaging*, vol. 14, no. 7/8, pp. 827-831, 1996.

Appendix

Energy Dispersive Spectroscopy:

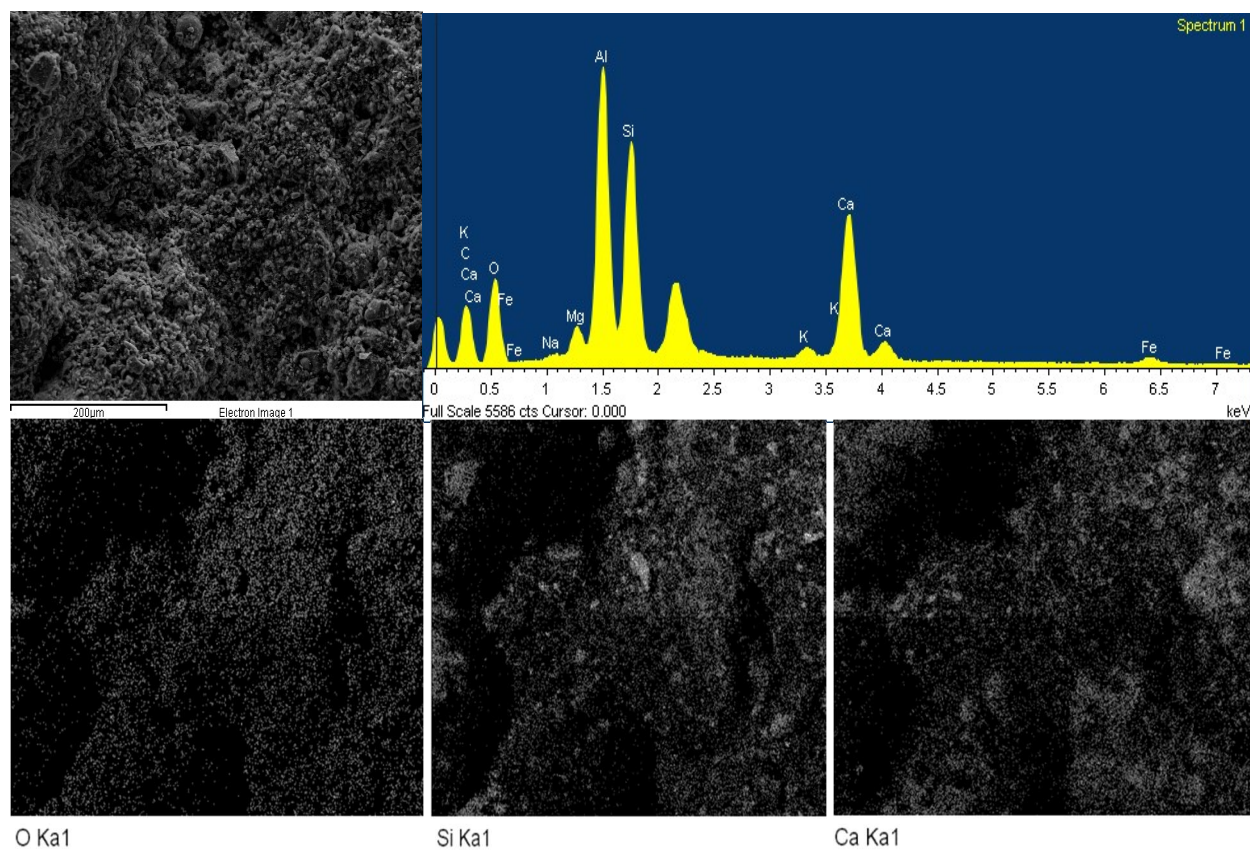
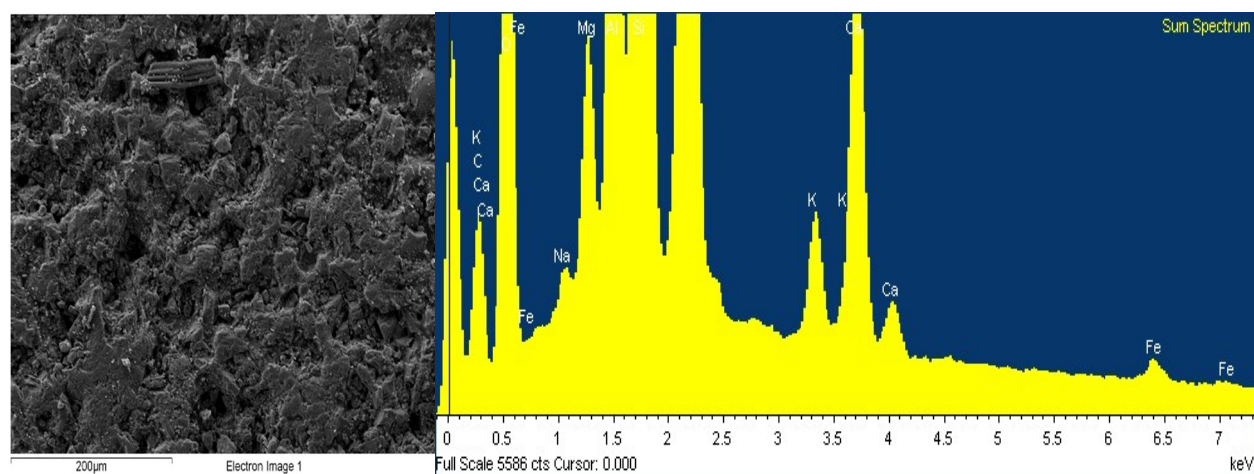


Fig A.1: EDS spectra and smart maps for 1-day sample



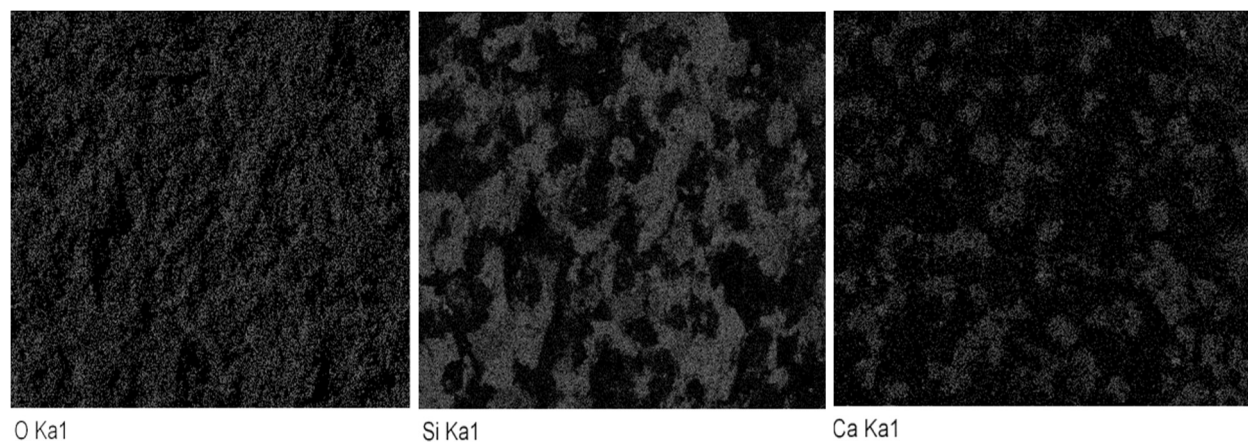


Fig A.2: EDS spectrum and smart maps for 2-days sample

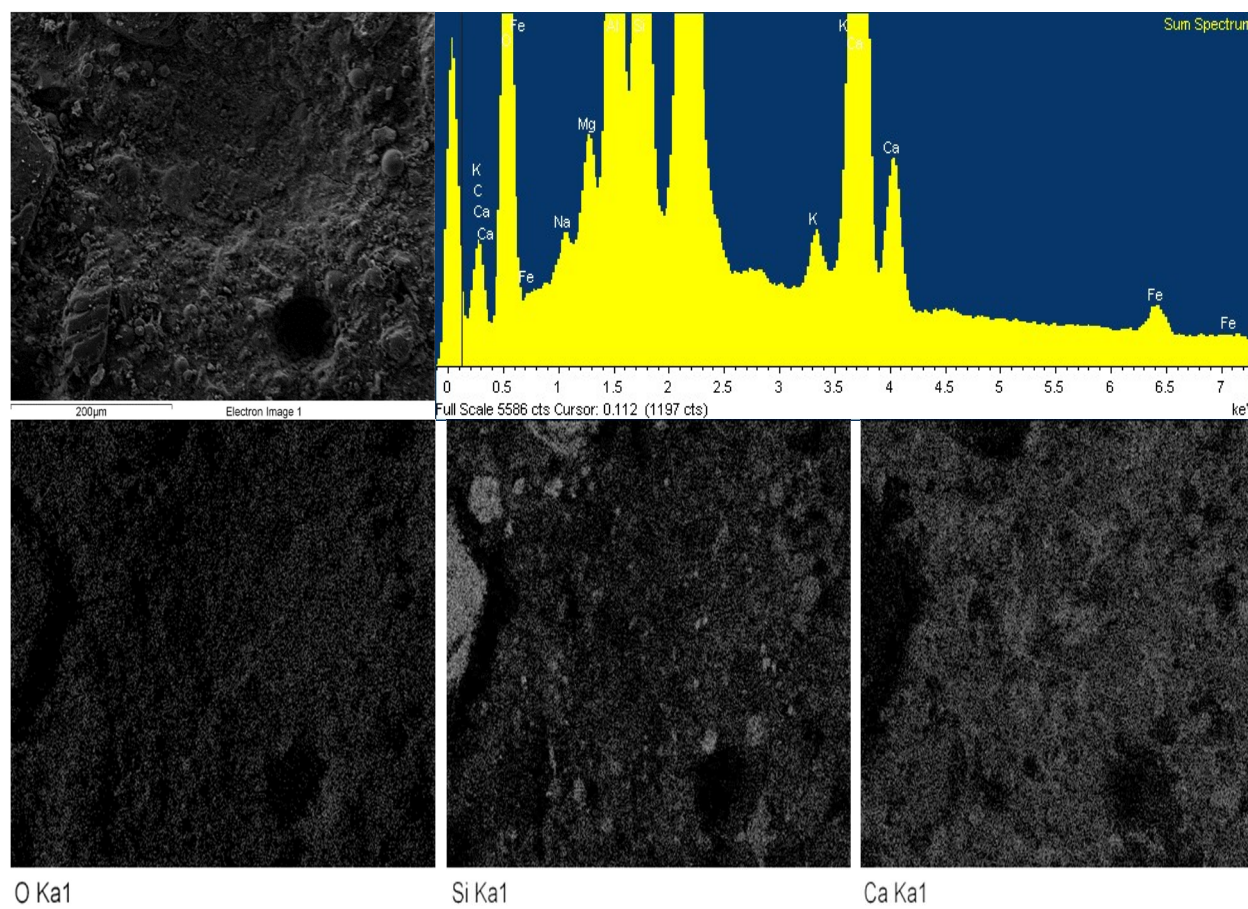


Fig A.3: EDS spectrum and smart maps for 3-days sample

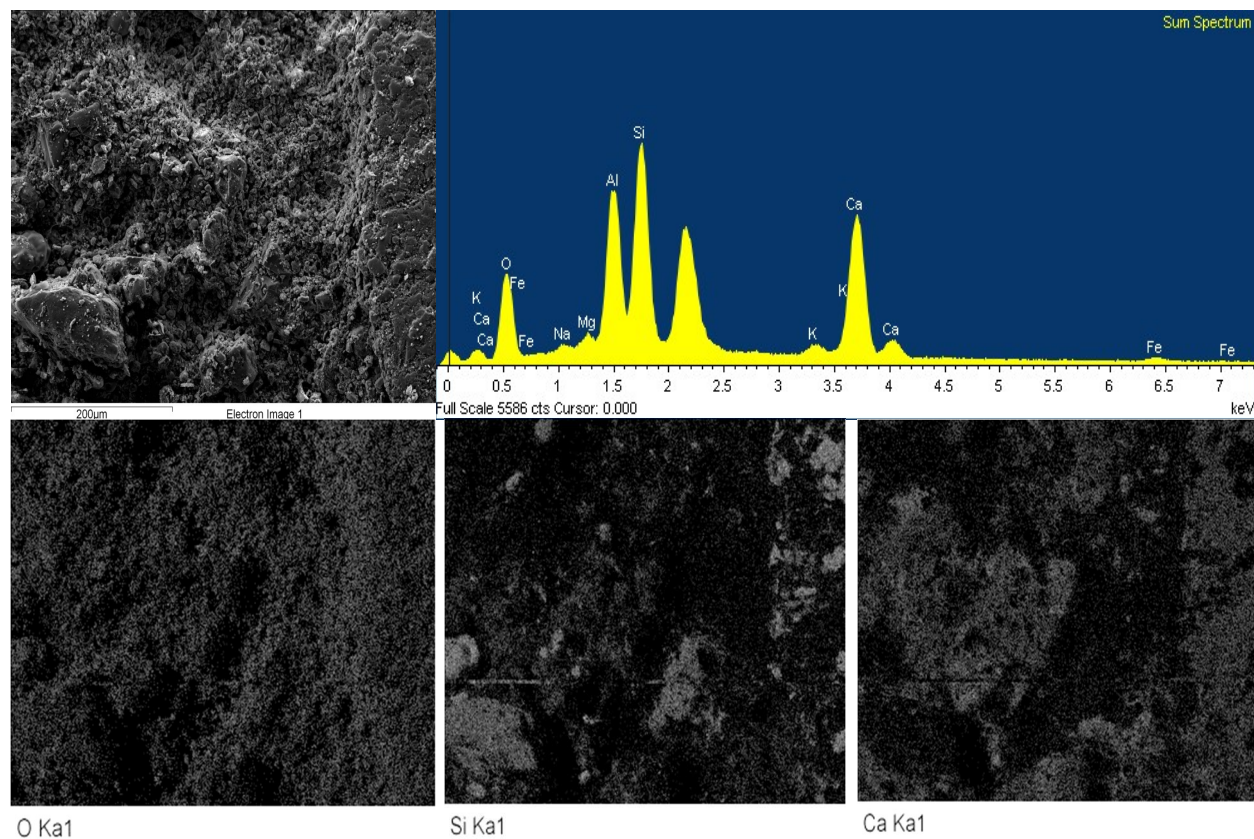


Fig A.4: EDS spectrum and smart maps for 4-days sample

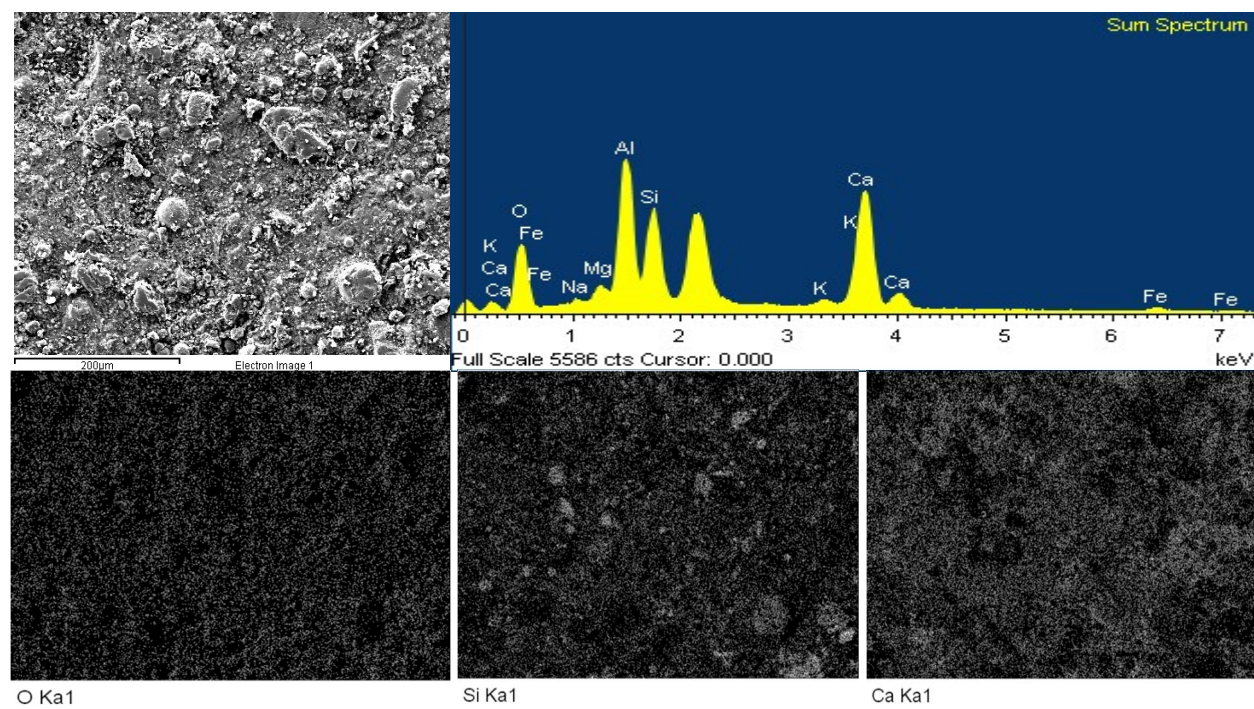


Fig A.5: EDS spectrum and smart maps for 5-days sample

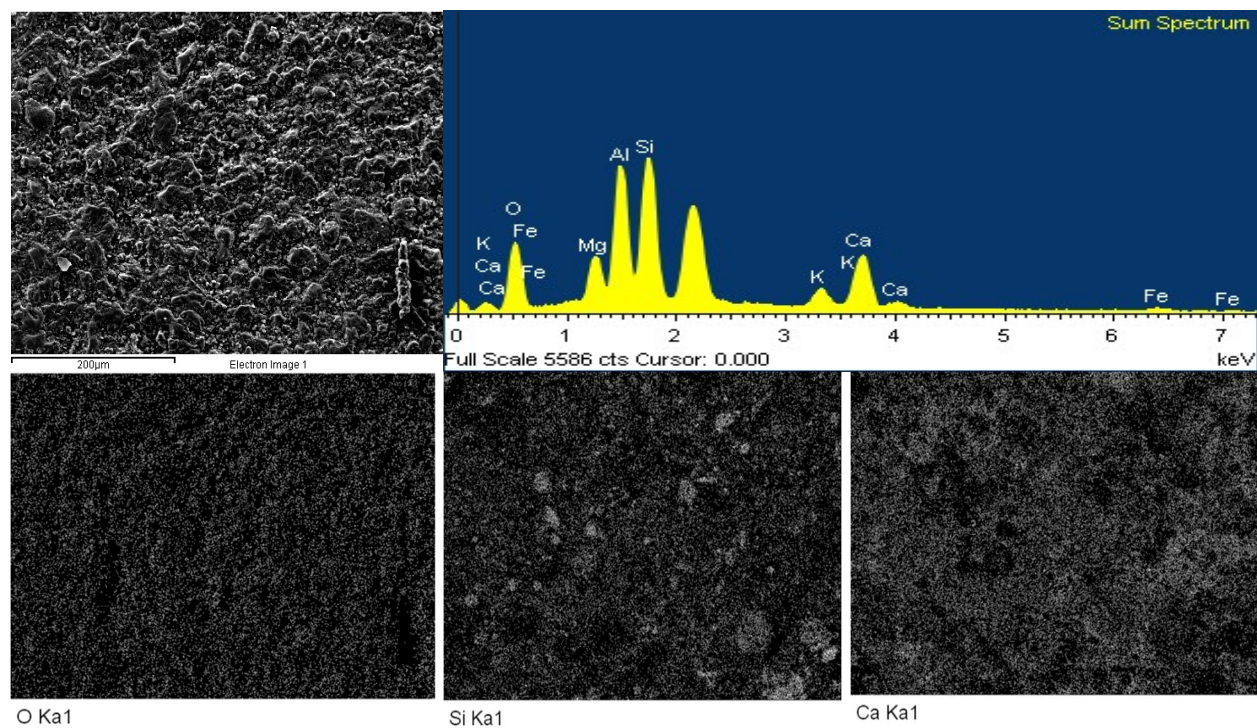


Fig A.6: EDS spectrum and smart maps for 7-days sample

Structure factor plot:

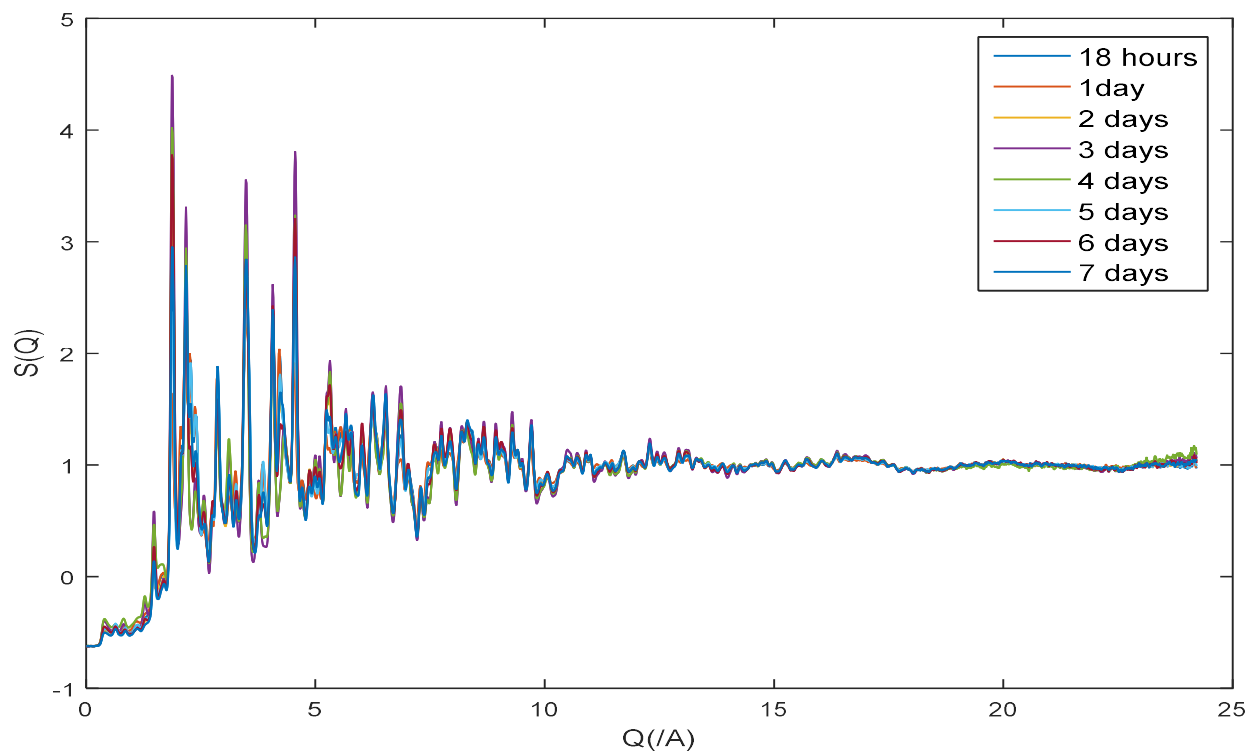


Fig A.7: Structure Factor, $S(Q)$, plots for different hydration times from PDF experiment

^{29}Si Nuclear Magnetic Resonance Report:

Detailed report of solid state ^{29}Si NMR for both white cement and synthetic C-S-H are shown below.

Report No: 118297v1
Date Issued: January 6, 2017

```

NAME      118297gadde.301
EXPHO    10
PROCNO    1
Date      20161212
Time      9.50
INSTRUM   spect
PROBHD    7 mm MAS 15N/3
PULPROG   hpdec.av
TD        324
SOLVENT   Acetone
NS        8127
DS        0
SWH       17857.143 Hz
FIDRES    55.114639 Hz
AQ        0.0091220 sec
RG        2050
DW        28.000 usec
DE        8.00 usec
TE        673.2 K
D1        10.0000000 sec
ZGPTNS    +Diacq
  
```

```

----- CHANNEL f1 -----
NUC1      2981
P1        3.50 usec
PLL       -2.90 dB
PL1W      235.09384155 W
SFO1      59.6229159 MHz
  
```

```

----- CHANNEL f2 -----
CPOPRG2   spinal64
NUC2      1H
P30       3.00 usec
P31       6.50 usec
PL2       120.00 dB
PL12      0.00 dB
PL2W      0.00000000 W
PL12W     86.66007996 W
SFO2      300.1320000 MHz
SI        2048
SF        59.6267705 MHz
WDW       EM
SSB       0
LB        100.00 Hz
GB        0
PC        0.20
  
```

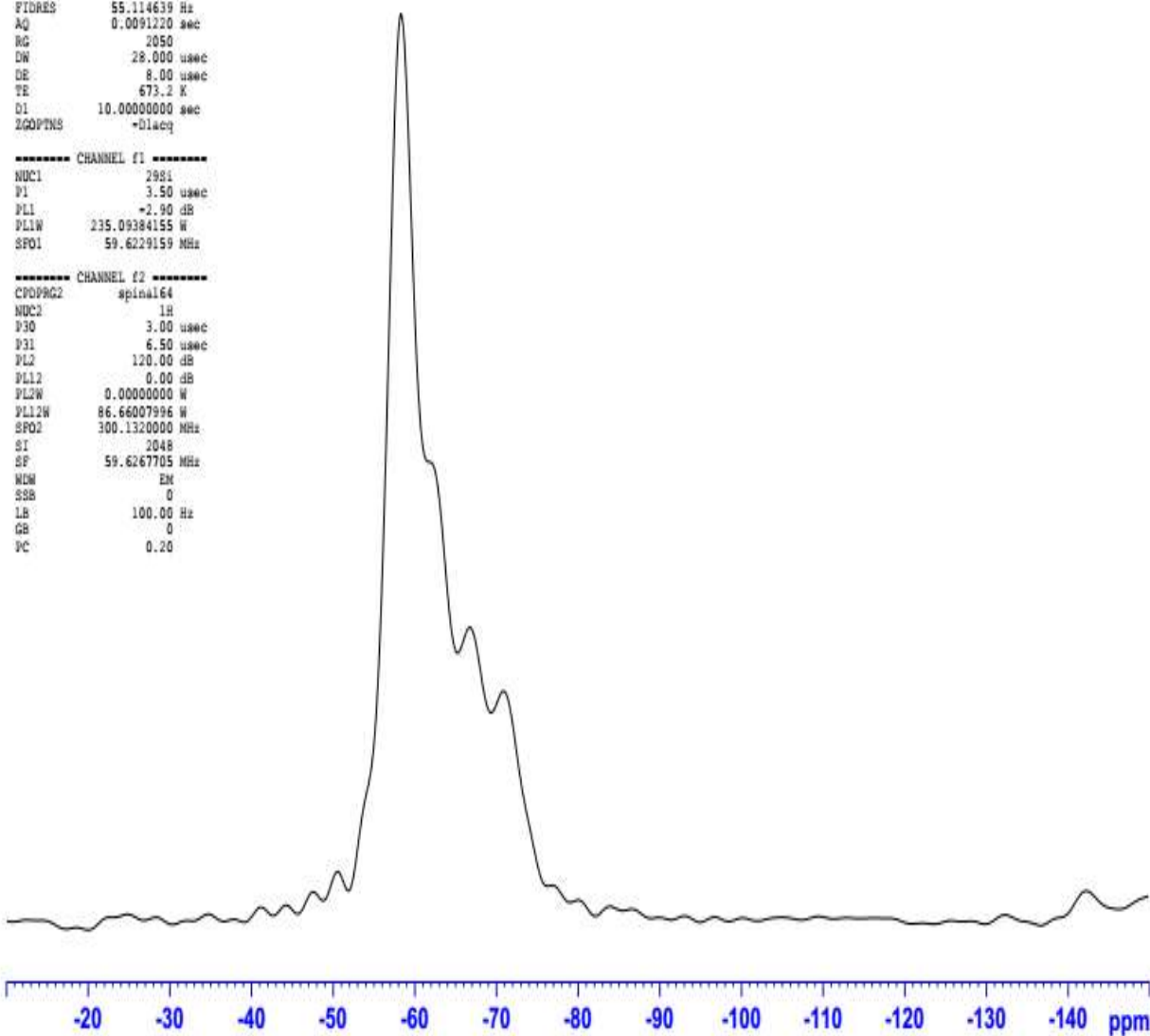


Figure 1. Solid state ^{29}Si NMR spectrum of WCP-1.

Fig A.8: NMR spectra for white cement paste confined in 0.0435" kapton tube

Report No: 118297v1
Date Issued: January 6, 2017

NAME 118297gadde.302
EXPMO 10
PROCNO 1
Date 20161213
Time 13.59
INSTRUM spect
PROBHD 7 mm MAS 15N/3
PULPROG hpcac.av
TD 324
SOLVENT Acetone
NS 8127
DS 0
SWH 17857.143 Hz
FIDRES 55.114639 Hz
AQ 0.0091220 sec
RG 2050
DW 28.000 usec
DE 8.00 usec
TE 673.2 K
D1 10.00000000 sec
ZGPPNS -Dlacc

----- CHANNEL f1 -----
NUC1 2981
P1 3.50 usec
PL1 -2.90 dB
PL1W 235.09384155 W
SFO1 59.6229159 MHz

----- CHANNEL f2 -----
CPOPRG2 apinal64
NUC2 1H
P30 3.00 usec
P31 6.50 usec
PL2 120.00 dB
PL12 0.00 dB
PL2W 0.00000000 W
PL12W 86.66007996 W
SFO2 300.1320000 MHz
SI 2048
SF 59.6267705 MHz
WDW EM
SSB 0
LB 100.00 Hz
GB 0
PC 0.20

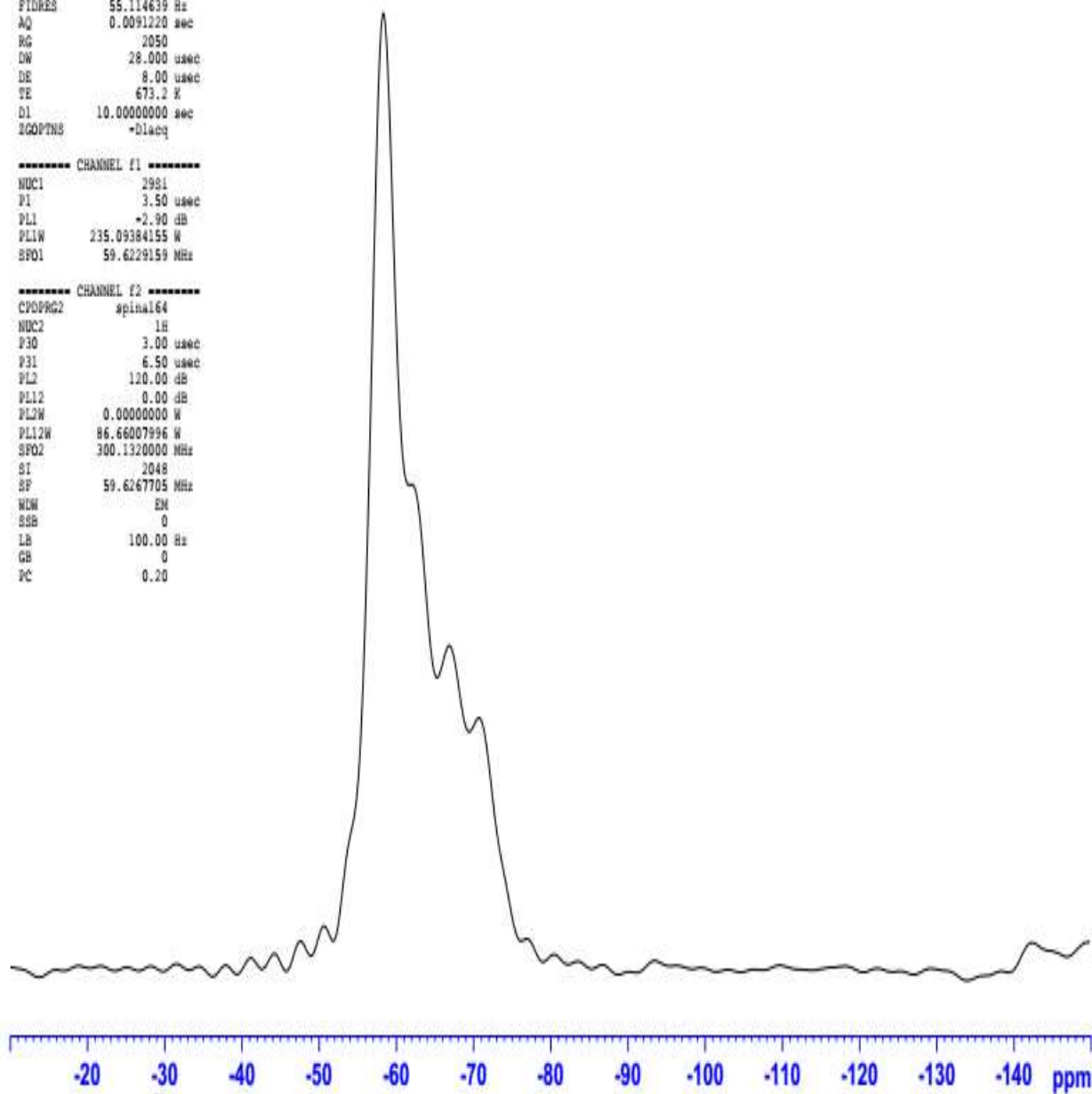


Figure 2. Solid state ^{29}Si NMR spectrum of WCP-2.

Fig A.9: NMR spectra for white cement paste confined in 0.0270" kapton tube

Report No: 118297v1
Date Issued: January 6, 2017

NAME 118297gadde.303
EXPNO 10
PROCNO 1
Date_ 20161223
Time_ 10.01
INSTRUM spect
PROBHD 7 mm MAS 15N/3
PULPROG hpdec.av
TD 324
SOLVENT CDCl3
NS 8127
DS 0
SWH 17857.143 Hz
FIDRES 55.114639 Hz
AQ 0.0091220 sec
RG 2050
DW 28.000 usec
DE 8.00 usec
TE 673.2 K
D1 10.00000000 sec
ECOPTNS -D1acq

----- CHANNEL f1 -----
NUC1 2981
P1 3.50 usec
PL1 -2.90 dB
PL1W 235.09384155 W
SFO1 59.6229159 MHz

----- CHANNEL f2 -----
CPDPRG2 spinal64
NUC2 1H
P30 3.00 usec
P31 6.50 usec
PL2 120.00 dB
PL12 0.00 dB
PL2W 0.00000000 W
PL12W 86.66007996 W
SFO2 300.1320000 MHz
SI 2048
SF 59.6267705 MHz
NDW EM
SBB 0
LB 100.00 Hz
GB 0
PC 0.20

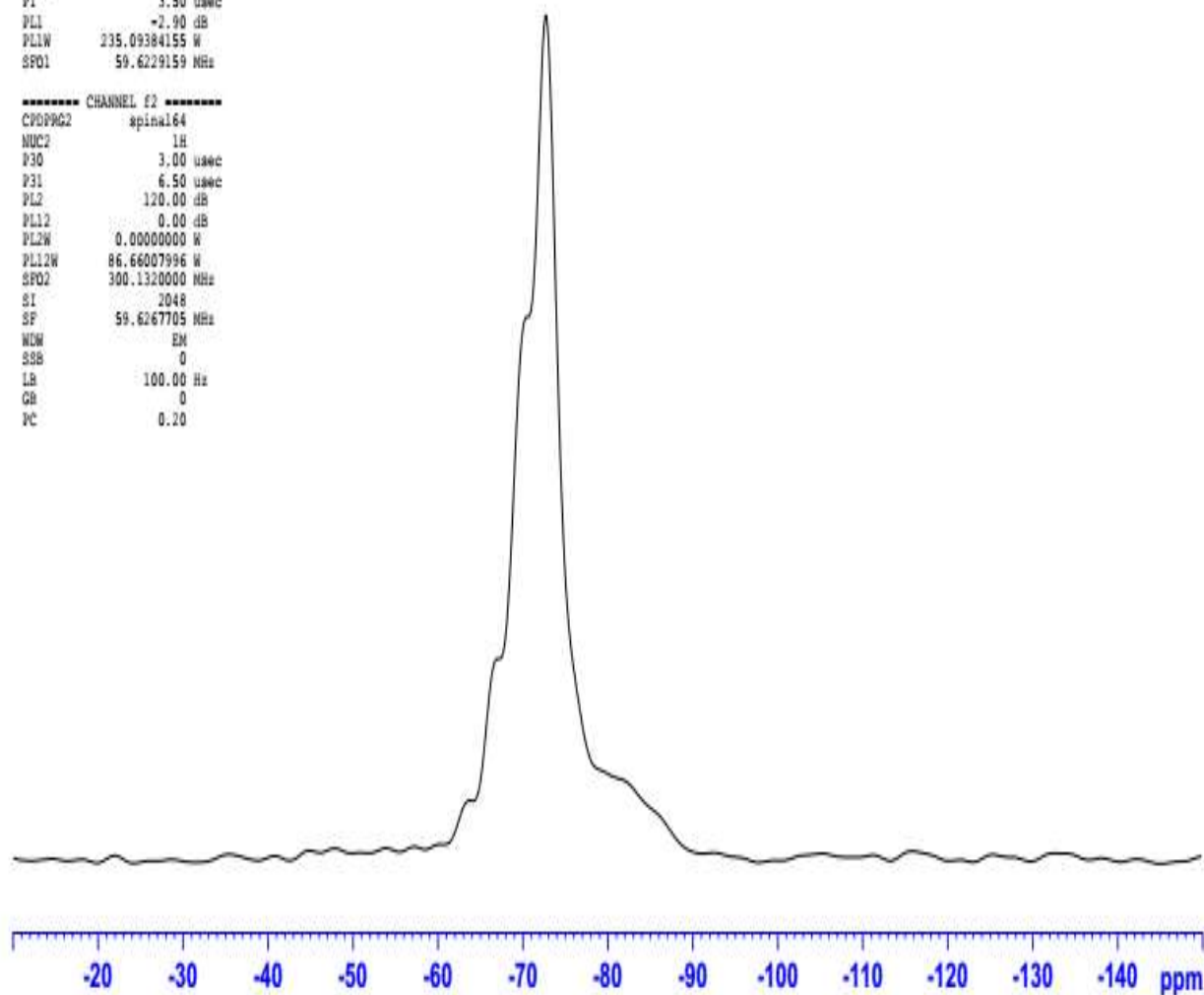


Figure 3. Solid state ^{29}Si NMR spectrum of CSH-1.

Fig A.10: NMR spectra for synthetic C-S-H confined in 0.0435" kapton tube

Report No: 118297v1
Date Issued: January 6, 2017

```

NAME      118297gadde.304
EXPNO     10
PROCNO    1
Date_     20161227
Time      16.19
INSTRUM   spect
PROBHD    7 mm MAS 15N/3
PULPROG   hpdec.av
TD         324
SOLVENT   CDC13
NS         8127
DS         0
SWH       17857.143 Hz
FIDRES    55.114639 Hz
AQ         0.0091220 sec
RG         2050
DW         28.000 usec
DE         8.00 usec
TE         673.2 K
D1         10.0000000 sec
ZGPPRMS   -0.1acq

```

```

----- CHANNEL f1 -----
NUC1      29Si
P1        3.50 usec
PL1       -2.90 dB
PL1W      235.09384155 W
SFO1      59.6229159 MHz

```

```

----- CHANNEL f2 -----
CPOPRG2   spina164
NUC2       1H
P30        3.00 usec
P31        6.50 usec
PL2        120.00 dB
PL12       0.00 dB
PL2W       0.00000000 W
PL12W      86.66007996 W
SFO2      300.1320000 MHz
SI         2048
SF         59.6267705 MHz
NUC3       EM
SBB         0
LB         100.00 Hz
GB         0
PC         0.20

```

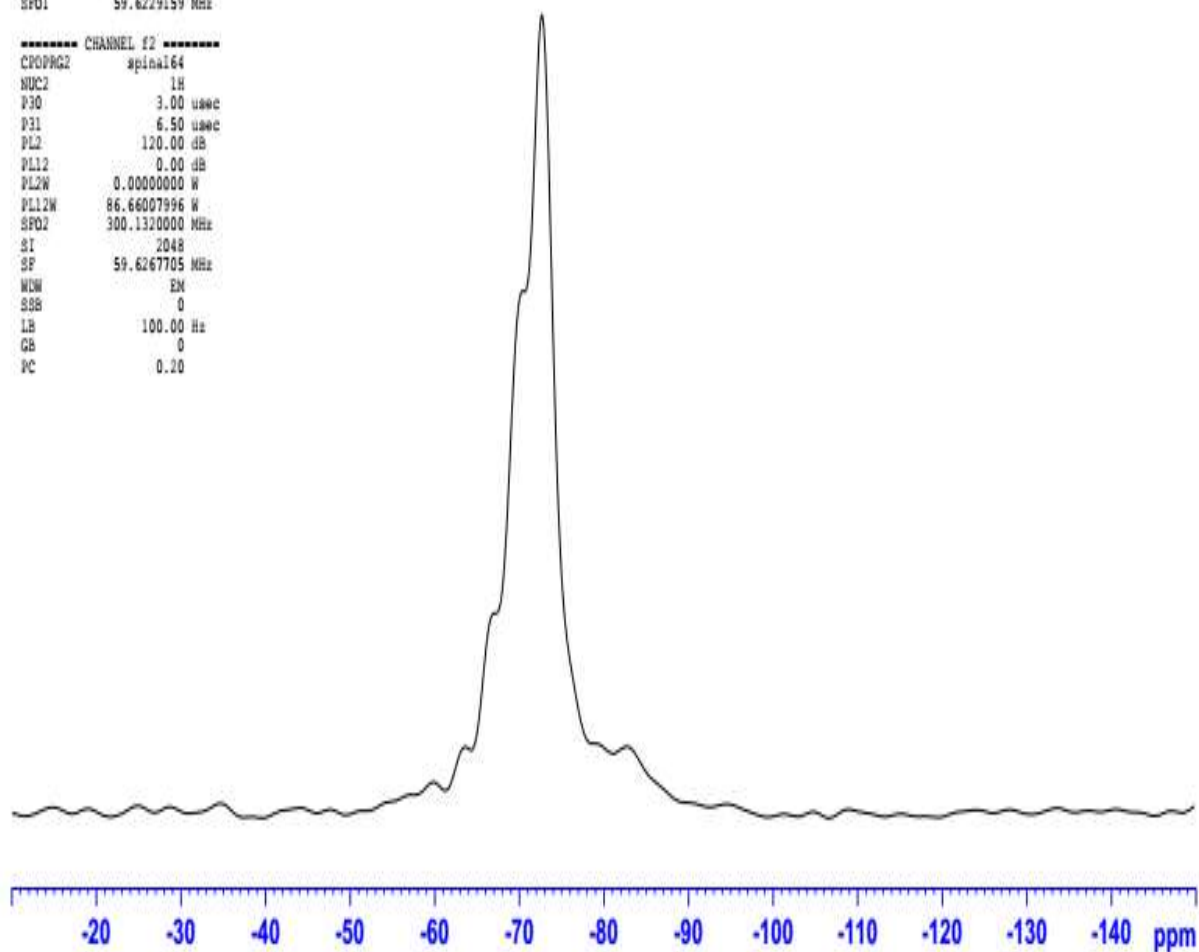


Figure 4. Solid state ^{29}Si NMR spectrum of CSH-2.

Fig A.11: NMR spectra for synthetic C-S-H confined in 0.0270" kapton tube